Molecular Therapy
Methods & Clinical Development
Original Article

Neuroglobin Can Prevent or Reverse Glaucomatous Progression in DBA/2J Mice

Hélène Cwerman-Thibault,[1,2,9] Christophe Lechauve,[1,3,9] Sébastien Augustin,[1] Delphine Roussel,[1,4] Élodie Reboussin,[1] Ammara Mohammad,[1,5] Julie Degardin-Chicaud,[1] Manuel Simonutti,[1] Hong Liang,[1,6] Françoise Brignole-Baudouin,[1] Anne Maron,[7] Thomas Debeir,[8] and Marisol Corral-Debrinski[1,2]

[1]Sorbonne Universités, UPMC Univ Paris 06, INSERM, CNRS, Institut de la Vision, 17 rue Moreau, 75012 Paris, France; [2]PROTECT, INSERM, Université Paris Diderot, Sorbonne Paris Cité, 75019 Paris, France; [3]Department of Hematology, St. Jude Children's Research Hospital, Memphis, TN 38105, USA; [4]Institut du Cerveau et de la Moelle Épinière, Hôpital Pitié Salpêtrière, 75013 Paris, France; [5]Genomic Paris Centre, Institut de Biologie de l'Ecole normale supérieure, 46 rue d'Ulm, 75230 Paris, France; [6]CHNO des Quinze-Vingts, DHU Sight Restore, INSERM-DHOS CIC, 28 rue de Charenton, 75012 Paris, France; [7]Sanofi-Aventis, 94400 Vitry-sur-Seine, France; [8]Departments of Evaluation and Expertise Strategy, Science Policy and External Innovation, Sanofi, 75008 Paris, France

Mitochondrial dysfunction is responsible for hereditary optic neuropathies. We wished to determine whether preserving mitochondrial bioenergetics could prevent optic neuropathy in a reliable model of glaucoma. DBA/2J mice exhibit elevated intraocular pressure, progressive degeneration of their retinal ganglion cells, and optic neuropathy that resembles glaucoma. We established that glaucoma in these mice is directly associated with mitochondrial dysfunction: respiratory chain activity was compromised in optic nerves 5 months before neuronal loss began, and the amounts of some mitochondrial proteins were reduced in retinas of glaucomatous mice. One of these proteins is neuroglobin, which has a neuroprotective function. Therefore, we investigated whether gene therapy aimed at restoring neuroglobin levels in the retina via ocular administration of an adeno-associated viral vector could reduce neuronal degeneration. The approach of treating 2-month-old mice impeded glaucoma development: few neurons died and respiratory chain activity and visual cortex activity were comparable to those in young, asymptomatic mice. When the treatment was performed in 8-month-old mice, the surviving neurons acquired new morphologic and functional properties, leading to the preservation of visual cortex activity and respiratory chain activity. The beneficial effects of neuroglobin in DBA/2J retinas confirm this protein to be a promising candidate for treating glaucoma.

INTRODUCTION

Glaucoma is a neurodegenerative disease of the optic nerve (ON) that is characterized by the loss of retinal ganglion cell (RGC) somas and axons. In 2013, it was estimated that approximately 65 million people had glaucoma, making it the leading cause of blindness in the world.[1] An array of pathologic events appears to contribute to glaucoma: (1) the blockade of ON axonal transport, which decreases the supply of neurotrophic factors to RGCs and could trigger apoptosis;[2] (2) an insufficient ocular blood supply, attributable to elevated intraocular pressure (IOP) or vascular abnormalities;[3] (3) the high level of extracellular glutamate released by dying cells;[4] (4) excessive gliosis, which results in the discharge of toxic substances;[5] and (5) the overproduction of reactive oxygen species (ROS) and the subsequent oxidative stress generated in the trabecular meshwork (TM) (which is involved in aqueous humor drainage), glial cells, inner retina, or ON.[6]

The development of satisfactory therapies for glaucoma has been hindered by the incomplete elucidation of the molecular mechanisms that lead to the condition.[7,8] The results of several recent studies have suggested that mitochondrial dysfunction could be a key player in the pathogenesis of glaucoma, because RGCs are highly sensitive to impairment of their energy supply. This is probably due to their atypical structure; inside the eye, their axons lack myelin sheaths, which implies an extremely high energy requirement for generating and propagating action potentials. Mitochondrial dysfunction is responsible for hereditary optic atrophies such as Leber hereditary optic neuropathy and dominant optic atrophy, which also result in RGC loss and ON dysfunction leading to vision loss.[9] In primary open-angle glaucoma, the activity of respiratory chain complex I (CI) is reduced in patient lymphoblasts[10] and fibroblasts.[11] Lascaratos and colleagues[12] demonstrated that healthy mitochondria efficiently prevent glaucomatous optic neuropathy in patients who have exhibited elevated IOP for many years. Accordingly, therapeutic approaches aimed at preserving mitochondrial integrity could sustain visual function in patients by protecting their RGCs against degeneration.[13]

Since 2009, we have investigated the function of neuroglobin in mitochondria. This protein of 151 amino acids, identified in vertebrates as a member of the globin superfamily, is abundant in various regions of the brain and in the eye[14] and is considered a powerful neuroprotectant.[15]

Received 26 October 2016; accepted 21 April 2017;
http://dx.doi.org/10.1016/j.omtm.2017.04.008.

[9]These authors contributed equally to this work.

Correspondence: Marisol Corral-Debrinski, PROTECT, INSERM (UMR1141), Université Paris Diderot, Sorbonne Paris Cité, 48 Boulevard Sérurier, 75019 Paris, France.
E-mail: marisol.corral@inserm.fr

We previously showed that rodent RGCs[16] and ONs[17] possess high levels of neuroglobin (NGB). We also demonstrated that NGB was enriched in mitochondrial fractions and that knock down of the *Ngb* gene in rat RGCs caused cell death, optic neuropathy, and defects in respiratory CI and III that led to visual function impairment.[18] Harlequin mice exhibit optic neuropathy caused by the depletion of the mitochondrial apoptosis-inducing factor (AIF), leading to respiratory chain impairment.[19] A 2-fold decrease in the steady-state levels of NGB was observed in retinas from these mice; hence, ocular gene therapy mediated by an adeno-associated viral vector serotype 2 (AAV2/2) driving the synthesis of NGB (AAV2/2-*NGB*) was performed before the onset of optic atrophy. This approach prevented RGC loss and preserved respiratory chain activity in ONs and visual function.[20]

Our current objective is to increase our understanding of the link between mitochondrial impairment and glaucoma and to develop a therapeutic approach that uses NGB, with the aim of preserving organelle integrity in an experimental model of glaucoma. The DBA/2J mouse strain exhibits iris atrophy and elevated IOP due to the release of pigment clumps into the anterior chamber of the eye.[21,22] In these mice, RGC degeneration, optic neuropathy, and a visual function deficit are evident by the age of 12 months.[23,24] We demonstrated that mitochondrial dysfunction in the retina and ON precedes the development of the glaucomatous phenotype in DBA/2J mice. Administering AAV2/2-*NGB* to mice several months before the onset of RGC degeneration leads to increased abundance of NGB in the retinas, which strongly correlates with the preservation of ON morphology and function. Moreover, when NGB therapy is administered after neuronal loss has already begun, the surviving neurons are able to enhance visual cortical function via morphologic changes within the retina and the preservation of respiratory chain activity in the ONs.

RESULTS

Assessment of Anterior-Segment Eye Morphology and Intraocular Pressure in DBA/2J Mice

To define iris pathology and corneal changes, we examined DBA/2J mice aged 2 to 12 months by in vivo confocal microscopy (Figure 1A). The eyes of 4-month-old mice had normal superficial epithelium and stroma, with scattered hyperreflective patterns in the endothelium. Additionally, at this age, the iris contained numerous filamentous and hyperreflective aggregates (Figure 1A, panel J, white arrowhead). The degenerative process in both the cornea and iris became aggravated 4 months later: we observed activated keratocytes with a stellar shape in the stroma (Figure 1A, panel M, black arrowhead); the density of hyperreflective dots and pigment clumps increased in the endothelial layers (Figure 1A, panel N, black arrowhead); and it was difficult to visualize the iris because of the presence of numerous pigment clumps among the inflammatory cells (Figure 1A, O, white arrowhead). The 1-year-old mice showed corneal epitheliopathy, with numerous dark microcysts (round vesicles containing fluid and cellular debris) and epithelial cells with disrupted morphology. The other corneal layers also exhibited pathologic changes: the basal epithelium was abnormal, with many dense and hyperreflective polyhedral structures; the stroma exhibited holes and nearby fibrotic reactions (Figure 1A, R, black arrowhead); and the endothelial layer included numerous hyperreflective pigment clumps (Figure 1A, S, white arrowhead). The irises of 1-year-old mice contained fewer pigment clumps than did the irises of 8-month-old mice. To determine whether the progressive iris disease correlated with ocular hypertension, we measured the IOP in DBA/2J mice aged between 2 and 14 months (Figure 1B). The IOP of DBA/2J mice increased from the age of 7 months and reached a maximum in 11-month-old mice. Thereafter, ocular hypertension declined progressively, reaching the baseline in 14-month-old mice (Figure 1B). Figure 1B also shows the IOP in C57BL/6J mice at various ages. The congenic C57BL/6J strain is considered a control for DBA/2J mice, as C57BL/6J mice lack the mutations in the *Gpnmb* and *Tyrp1b* genes that are responsible for iris pathology.[21,25] No significant changes in IOP were observed in these mice, with the mean values being between 13 mm Hg (in 2- and 8-month-old mice) and 11.8 mm Hg (in 14-month-old mice). Hence, the fibrosis and inflammation in the corneas and irises noticed at first in DBA/2J mice aged 4 months and which aggravate progressively up to 1 year appeared to be correlated with changes in IOP and might contribute to the subsequent neuronal loss in the inner retina, as previously described.[26]

Evaluation of Retinal Ganglion Cell and ON Degeneration in DBA/2J Mice

Retinal sections from mice aged between 2 and 15 months were immunolabeled with an antibody against BRN3A, a transcription factor that accumulates in most RGCs in rodent retinas.[27] It has been reported that DBA/2J mice aged 2 to 4 months do not exhibit signs of retinal degeneration; the earliest detectable changes occur at 8 to 10 months of age, with the number of animals showing degeneration reaching a peak by 11 to 12 months of age.[23,28–30] Therefore, we compared the RGC population in groups of DBA/2J mice aged between 2 and 15 months (Figure 2). There were 13 retinas from 8-month-old mice that were evaluated, of which only two showed a decrease (of 30% and 35%) in the number of RGCs relative to that in 2-month-old mice. Conversely, in 58 retinas from mice aged 10 months or older, there were noticeably fewer BRN3A-positive cells in the ganglion cell layer (GCL) when compared to the GCL of 2-month-old mice. The equivalent of 65% of the RGCs had disappeared in DBA/2J mice aged 10 months or older, as compared to 2-month-old mice, which is consistent with previous reports (Figures 2A and 2B).[23,28,29]

Retinal sections were also immunolabeled with an antibody against glial fibrillary acidic protein (GFAP), which is a sensitive marker for glial activation in astrocytes and Müller cells in response to a retinal stress.[31] Intense GFAP staining extending to the outer nuclear layer (ONL) was observed in retinas from 8- and 15-month-old mice, indicating that the amount of protein had increased in all Müller-cell compartments. The significantly increased intensity of GFAP staining in retinal sections from mice aged 8 months or older confirmed the activation of Müller cells and astrocytes in mouse retinas during glaucoma progression (Figures 2A, 2C, and S1).

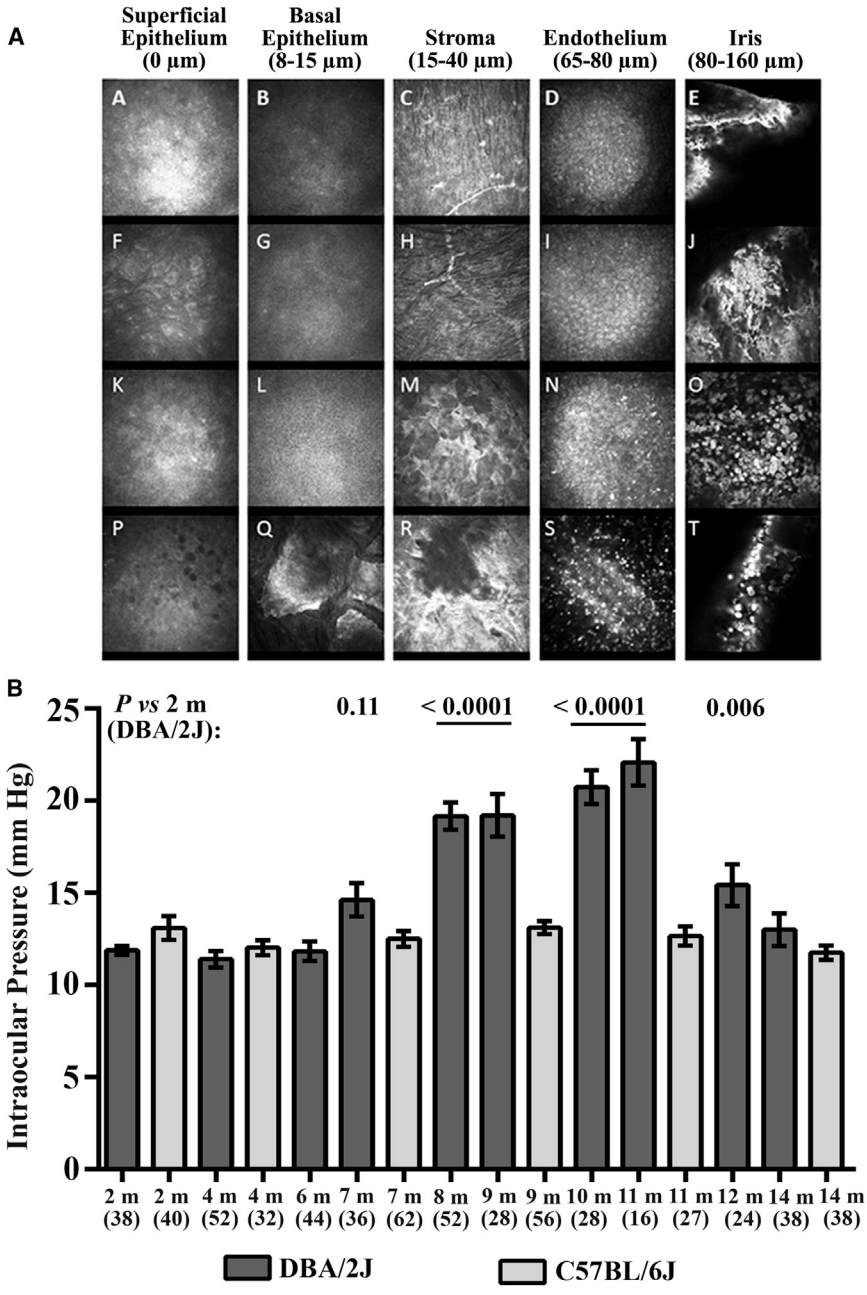

Figure 1. Anterior Segment and Intraocular Pressure Changes in DBA/2J Mice with Age

(A) In vivo confocal microscopy images of the anterior segments of DBA/2J mice, including the corneal superficial epithelium (column 1), basal epithelium (column 2), stroma (column 3), endothelium (column 4), and iris (column 5), for DBA/2J mice aged 2 months (row 1), 4 months (row 2), 8 months (row 3), and 12 months (row 4). For each age group, usually four mice were evaluated over time. The black and white arrowheads indicate changes in the cornea and the iris during aging. (B) Male DBA/2J and C57BL/6J mice aged between 2 and 14 months were subjected to noninvasive IOP measurements that were performed monthly on both eyes during daylight. The histogram shows the means ± SEMs, as well as the age in months (m) and the number of eyes evaluated in each group. Although IOP measurements can differ between the right and left eyes in some animals, the data shown did not discriminate between the values for individual eyes. The p values were calculated with respect to measurements collected from 2-month-old DBA/2J mice; only the values close to significance or significant are shown (for mice aged 7–12 months).

By using qRT-PCR, we evaluated the steady-state levels of *Brn3A* and *Gfap* mRNA in retinas from mice aged between 2 and 15 months. By the age of 12 months, *Brn3A* mRNA decreased by approximately 75%, whereas *Gfap* mRNA increased by 300% relative to the amount detected in retinas from 2-month-old mice (Figures S2A and S2B). Moreover, 15-month-old DBA/2J mice exhibited a reduction in the thickness of the ONL and inner nuclear layer (INL) relative to the corresponding layers in 2-month-old DBA2/J mice and 15-month-old C57BL/6J mice, indicating that the change was not age related (Figure S3). These data are consistent with a recent report that cell loss is not limited to the GCL in advanced stages of the disease.[32]

Next, we estimated the extent of RGC axonal disappearance in sections of ONs from DBA/2J mice by using antibodies against the heavy-chain subunit of neurofilaments (NF200). Figure 3A shows a reduced number of immunopositive dots in the ONs of 12-month-old DBA/2J mice. Axonopathy was measured by counting NF200-positive spots (each spot represents a single nerve fiber) in mice aged 2, 8, or 12 months (Figure 3B). After the results were normalized against the average value for 2-month-old mice, 8-month-old mice exhibited an axonal loss of 33.3%, despite the survival at this age of RGC somas (equivalent to 89% of the RGCs in 2-month-old mice). Thereafter, the pathologic process became aggravated; 12-month-old mice retained only 22% of the optic fibers and approximately 35% of the RGC somas seen in 2-month-old mice.

We performed immunohistochemical staining on sections of ONs with antibodies against three markers: GFAP, ionized calcium-binding adaptor molecule 1 (IBA1), and vimentin (a cytoskeleton marker that is especially abundant in astrocytes). The antibodies against GFAP and vimentin yielded stronger signals with ONs from mice aged 8 or 12 months than with ONs from 2-month-old mice (Figures 3A and 3C); astrocytes probably replaced the axon bundles that

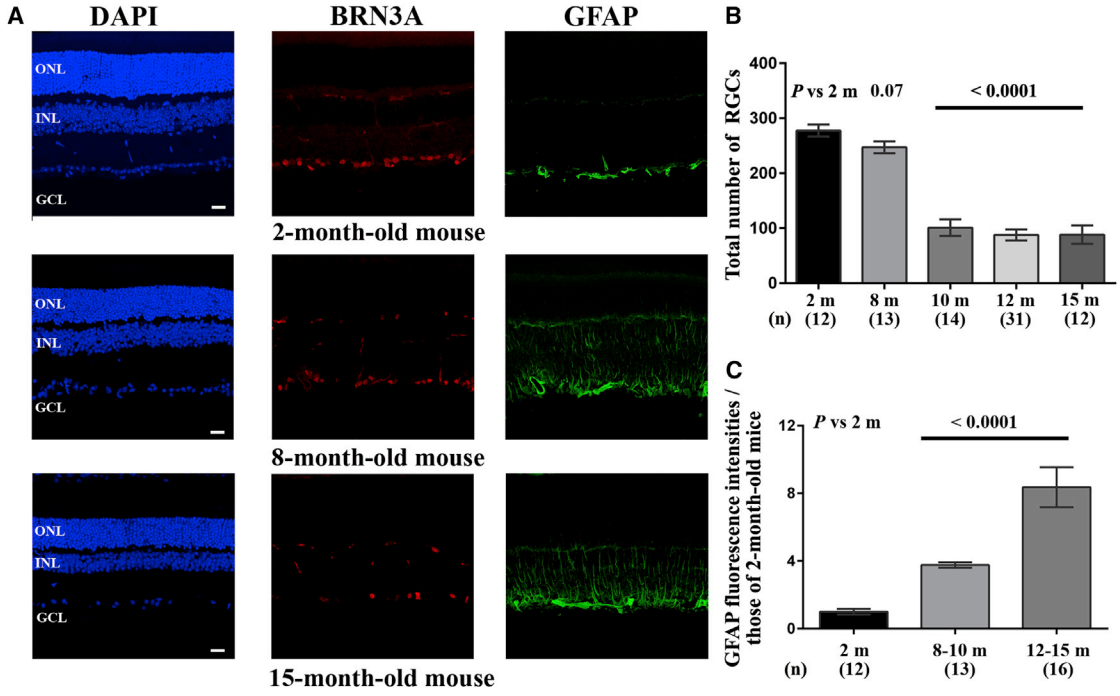

Figure 2. Ganglion Cell Loss and Gliosis in Retinas of DBA/2J Mice during the Progression of Glaucoma

(A) Immunohistochemical staining for BRN3A (red) and GFAP (green) in retinas from mice aged 2, 8, and 15 months; the nuclei were stained with DAPI (blue) for contrast. Abbreviations: ONL, outer nuclear layer; INL, inner nuclear layer; GCL, ganglion cell layer; OPL, outer plexiform layer; IPL, inner plexiform layer. The scale bar represents 20 μm. (B) The overall number of RGCs was estimated in DBA/2J mice of different ages by counting BRN3A-positive cells in the GCL after reconstructing retinal sections, as described in the Materials and Methods section. The histogram shows the number of RGCs as the mean ± SEM; the number of mice evaluated by age group in months (m) is shown in brackets (n) below each bar. (C) The intensity of the GFAP labeling was estimated with ImageJ in whole retinas from mice in the three age groups: 2 months (healthy), 8 to 10 months (with well-established glaucoma), and 12 to 15 months (with advanced glaucoma). The histogram illustrates the data for each age group; the number below each bar corresponds to the number of independent retinal sections evaluated per group (n). The p values in (B) and (C) were calculated with respect to data collected in 2-month-old DBA/2J mice; only the values close to significance or significant are shown.

disappeared progressively during glaucoma progression. We also saw more substantial IBA1 staining in ONs from mice aged 8 and 12 months than in ONs from young mice. The fluorescence intensity profiles calculated with ImageJ software for each antibody over the whole area of ON sections from mice aged 2, 8, and 12 months are shown in Figure 3D. The data suggest that activation of microglia and astrocytes in ONs occurred in 8-month-old mice, preceding the start of RGC loss by 2 months.

Respiratory Chain Activity in DBA/2J Retinas and ONs during Glaucoma Progression

We examined retinas and ONs from DBA/2J mice of various ages by a spectrophotometric method that assesses the enzymatic activities of respiratory chain complexes. Two independent assays were devised to sequentially measure the enzymatic activities of CI, CV, CIV, CII + CIII, and CIII in single-tissue homogenates.[33] Table 1 presents data obtained in DBA/2J retinas: CV enzymatic activity did not change with age, whereas a significant CI defect was evident in the retinas of mice aged 5 to 16 months when compared to retinas from 2-month-old mice; the reduction in CI activity reached approximately 50% in 10-month-old mice. Calculating the CI/CV ratios confirmed that there was a CI activity defect in DBA/2J mice aged 8 months or older, as compared to 2-month-old mice. The activities of CIV, CII + CIII, and CIII were also reduced in mice aged 10 months or 14 to 16 months when compared to the corresponding activities in 2-month-old mice (Table 1). For instance, CIII activity in mice aged 10 months or 14 to 16 months was severely diminished at 34% to 35% of the value measured in 2-month-old mice. Because the RGC population in rodent retinas accounts for only 1% of the total retinal neurons,[34] our results suggest that other retinal neurons exhibited compromised energetic metabolism. Furthermore, we observed a severe defect in all the complexes, except CV, in ONs. When mice aged 10 to 12 months were compared with 2-month-old mice, there were overall reductions of 60%, 48%, 45%, and 50% in the enzymatic activities of CI, CIV, CII + CIII, and CIII, respectively (Figure 4). Remarkably, ONs from 5-month-old mice also exhibited significant reductions in complex activities when compared to ONs from 2-month-old mice: the reductions were 47%, 55%, and 52% for CI, CIII, and CIV, respectively. Hence, bioenergetics failure in ONs from DBA/2J mice begins 5 months before RGC degeneration becomes measurable.

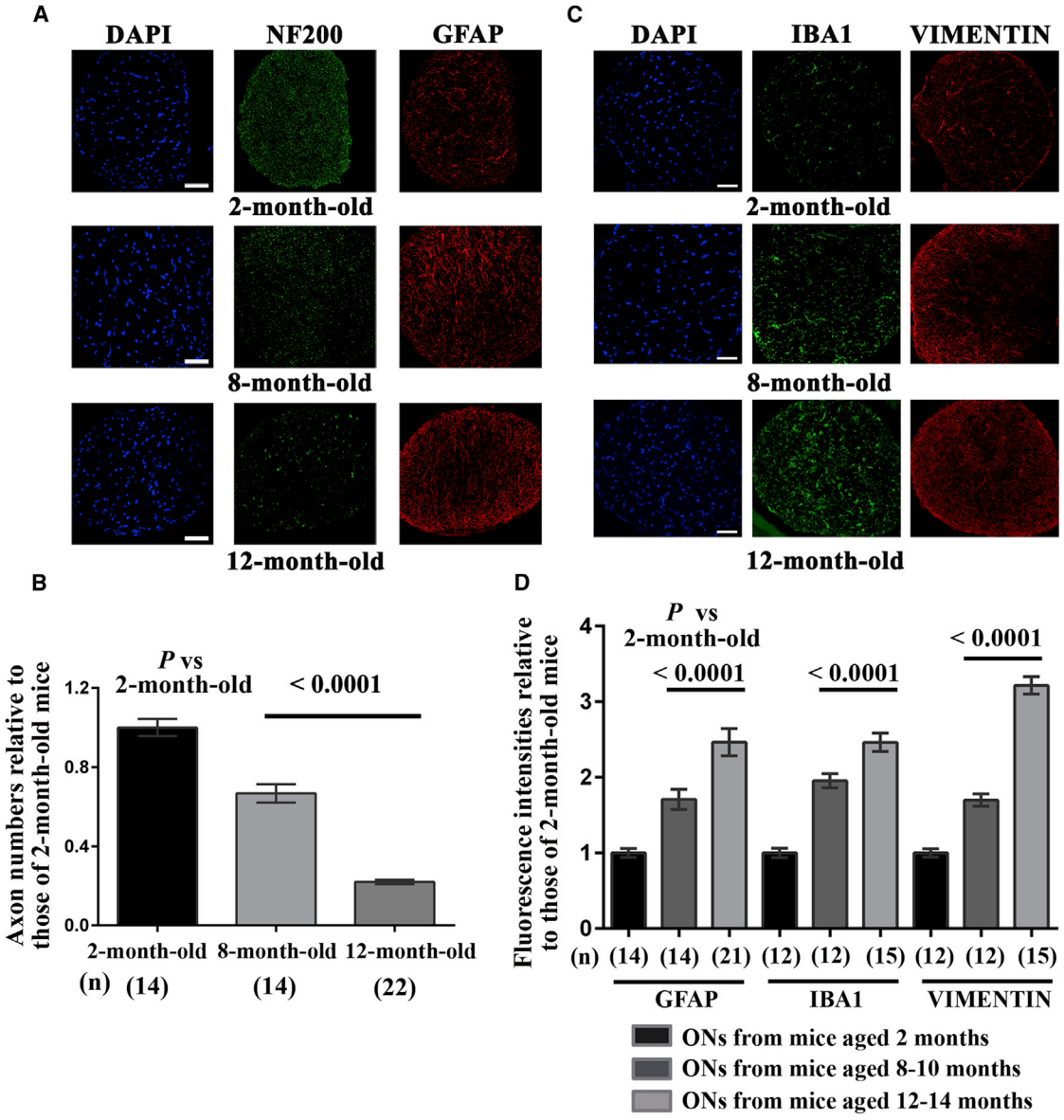

Figure 3. Histopathologic Changes in DBA/2J Optic Nerves over the Course of Disease

(A) Proximal ON transverse sections (near the globe) for mice aged 2, 8, and 12 months were subjected to immunohistochemical staining with antibodies against NF200 (green) and GFAP (an astrocyte marker) (red).(B) Bar graph of axon numbers (mean ± SEM) for optic nerves collected from mice aged 2, 8, and 12 months, as displayed with GraphPad Prism 6. The values are shown after normalization against those obtained from 2-month-old mice. NF200-positive spots were counted in three separate entire transverse sections with the ImageJ software. p values were calculated with respect to fiber number in 2-month-old DBA/2J mice; the number of mice evaluated (n) is shown in brackets below each bar of the histogram. (C) Immunohistochemical staining with antibodies against IBA1 (green) and vimentin (red). Both proteins were more abundant in ON sections from the older mice than in those from 2-month-old mice. The nuclei were stained with DAPI (blue) for contrast. The scale bar represents 50 μm for (A) and (C). (D) The bar chart illustrates the normalized values of the fluorescence intensities in ONs for GFAP, IBA1, and vimentin labeling as evaluated in mice at 2 months, 8 to 10 months, or 12 to 14 months of age. The results were normalized against the mean fluorescence in ONs from 2-month-old mice. The number of ON sections evaluated with ImageJ (n) is indicated in brackets below each bar corresponding to a specific age group. The values were plotted as means ± SEMs using GraphPad Prism 6.

Mitochondrial Protein Quantities in Retinas from Glaucomatous Mice

We evaluated the steady-state levels of several mitochondrial proteins in retinas from DBA/2J mice aged 2 months (the young group, Y) or 12 months (the old group, O). There were nine proteins involved in energetic metabolism, antioxidant defense, organelle morphology, or biosynthesis that were analyzed by western blotting, namely NDUFA9 (NADH:ubiquinone oxidoreductase subunit A9), ATP

Table 1. Respiratory Chain Complex Enzymatic Activities in Retinas of DBA/2J Mice

	Specific Activity ± SEM				
	2 Months	5 Months	8 Months	10 Months	14–16 Months
Complex I[a]	40.5 ± 1.9 (n = 26)[b]	32.14 ± 1.7 (n = 10)	31.8 ± 1.1 (n = 10)	21.5 ± 1.6 (n = 18)	24.7 ± 1.6 (n = 20)
p value versus 2-month-old mice		0.02	0.009	<0.0001	<0.0001
Complex V	103 ± 4.2 (n = 26)	96.7 ± 7.7 (n = 10)	102.8 ± 5.0 (n = 10)	94.8 ± 4.3 (n = 18)	97.1 ± 6.6 (n = 20)
p value versus 2-month-old mice		0.41	0.99	0.26	0.85
CI/CV	0.42 ± 0.03	0.36 ± 0.03	0.30 ± 0.02	0.24 ± 0.021	0.25 ± 0.016
p value versus 2-month-old mice		0.37	0.02	<0.0001	<0.0001
Complexes II + III[c]	48.5 ± 4.2 (n = 24)	ND	ND	30.3 ± 2.6 (n = 17)	24.3 ± 1.6 (n = 22)
p value versus 2-month-old mice				0.0055	<0.0001
Complex III[d]	247.9 ± 31.3 (n = 24)	ND	ND	86.1 ± 9.5 (n = 17)	82.9 ± 12.1 (n = 22)
p value versus 2-month-old mice				0.0007	<0.0001
Complex IV[e]	357.0 ± 9.7 (n = 24)	ND	ND	255.3 ± 19.4 (n = 17)	246.4 ± 13.97 (n = 22)
p value versus 2-month-old mice				<0.0001	<0.0001

[a]Complex I and complex V activities are expressed as nanomoles of oxidized "NADH/min/mg protein".
[b]The number of independent retinas evaluated is indicated in brackets.
[c]Complex II + III activity is expressed as nanomoles of reduced "cytochrome *c*/min/mg protein".
[d]Complex III activity is expressed as nanomoles of "oxidized decylubiquinone/min/mg protein".
[e]Complex IV activity is expressed as nanomoles of "oxidized cytochrome *c*/min/mg protein".

synthase subunit α, cytochrome *c* (Cyt-C), AIF, NGB, SOD2 (superoxide dismutase), HSP60 (heat shock protein 60), TOMM20 (translocation of outer mitochondrial membrane 20), and OPA1 (optic atrophy 1). In the old mice, the amounts of NDUFA9 (CI subunit), ATP synthase α (CV subunit), AIF, NGB, OPA1, and SOD2 reached 35.8%, 36.7%, 42%, 44%, 47%, and 49%, respectively, of the amounts measured in the young mice. The HSP60 and TOMM20 levels in the old mice were 66% and 82%, respectively, of those in the young animals, but these reductions were still significant ($p = 0.003$), whereas the abundance of Cyt-C was unchanged in the retinas evaluated. The abundance of GFAP was also measured in mice of both age groups, and the amount of GFAP was increased 2-fold in retinas from old mice, relative to retinas from 2-month-old mice, confirming that Müller cells and astrocytes underwent reactive changes correlated with RGC loss (Figures 5A and 5B).

We performed immunohistochemical staining of retinal sections with antibodies against mitochondrial proteins to strengthen the data on the differential accumulation of these proteins in young and old mice and also to define the staining pattern in each retinal cell layer (Figure 6). The immunoreactivities of NGB, OPA1, and SOD2 within the cytoplasm were similar; only weak signals were obtained in the ONL, probably because few mitochondria are present in that layer, whereas strong signals were obtained in the INL, the GCL, the inner plexiform layer (IPL), and the inner segment of photoreceptors (IS), indicative of the high density of mitochondria in those compartments.[35] In the INL, many cells exhibited labeling around the nucleus. The IPL showed consistent labeling; this layer contains a highly complex network of interconnecting dendrites and synaptic terminals involving bipolar, amacrine, horizontal, and retinal ganglion cells. The signal may correspond to an important density of mitochondria within this compartment. In old DBA/2J mice, all the retinal cell layers showed weaker fluorescent signals for these proteins (Figure 6), consistent with the results of western blot analyses (Figure 5). The reduced accumulation of several key mitochondrial proteins can alter organelle functionality and exacerbate RGC injury.

AAV2/2-*NGB* Delivery to the Vitreous of Mice at Two Stages of the Pathogenic Process

To establish whether restoring NGB levels in RGCs could prevent neuronal injury, gene therapy was performed by using a recombinant AAV2/2 vector encompassing the mouse *Ngb* open reading frame (ORF) in association with the full-length 5′ and 3′ UTRs (Figure S4A). We performed gene therapy in 2-month-old DBA/2J mice (the early treatment group) with the goal of preventing RGC loss and in 8-month-old mice (the late treatment group) to establish whether the course of the disease could be changed despite its having reached an advanced stage. Because *Ngb* sequences were inserted into the pAAV-*hrGFP* vector, we used the GFP to assess the transduction yield in the retinas of mice that received early treatment. Reconstructions of entire retinal sections from injected eyes clearly showed homogeneous and intense GFP labeling that was restricted to the GCL (Figure S4B). When seven mice that received early treatment were evaluated 10 months later, approximately 79% of their RGCs had accumulated GFP (the cells showed intense BRN3A and GFP signals), indicating both efficient cellular transduction and stable transgene expression (Figure S4C).

We next performed immunohistochemical staining for NGB on retinal sections, and the immunofluorescence signal was noticeably

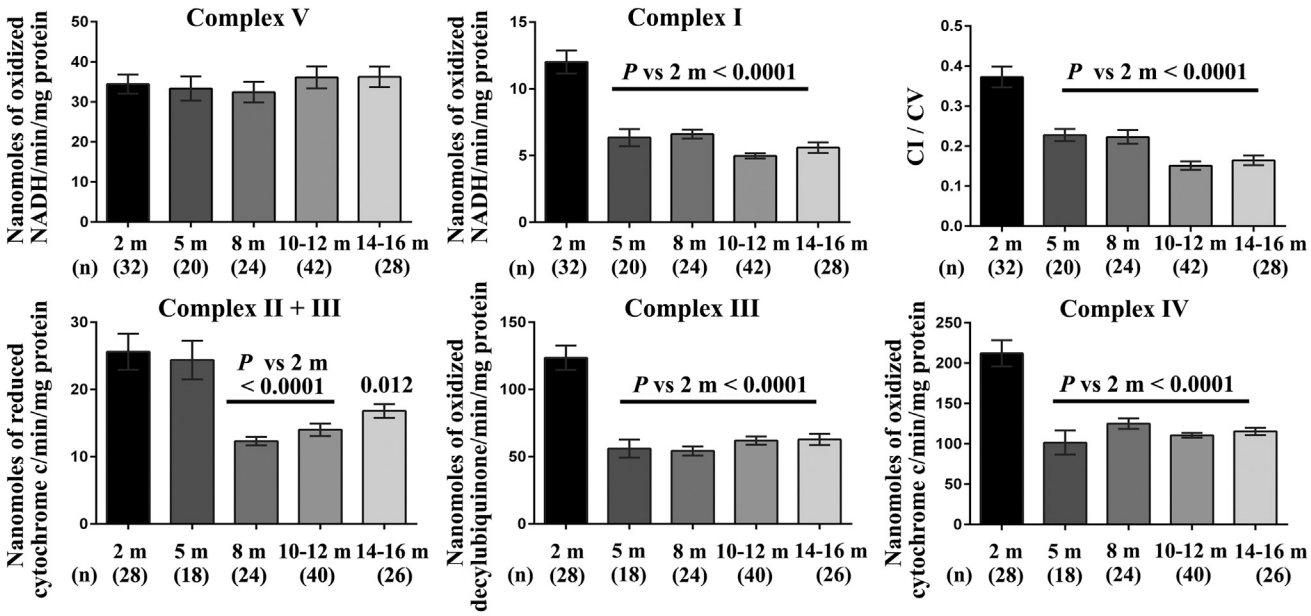

Figure 4. Respiratory Chain Activity in Optic Nerves from DBA/2J Mice at Various Ages

The enzymatic activities of complexes I, II + III, III, IV, and V were measured in single ONs isolated from DBA/2J mice of different ages, namely 2, 5, 8, 10 to 12, and 14 to 16 months. The values in each histogram represent the mean ± SEM of triplicates (CI and CV) or of duplicates (CII + CIII and CIII and CIV) for the samples evaluated; the CI/CV ratio is also shown. p values were calculated with respect to the activity assessed in 2-month-old DBA/2J mice. The age of the group in months (m) and the number of independent measurements performed is shown beneath each bar.

more intense in the GCL from a treated retina than in its untreated counterpart from a 12-month-old mouse (Figure S5A). Higher-magnification images of retinas from untreated mice aged 2 and 12 months and from mice after AAV2/2 administration are also shown in Figure S5B. The intensity of the NGB signal decreased with age, whereas in treated retinas, both the intensity and the number of positive cells increased. The punctuate labeling in cells exhibiting strong fluorescent signals was similar to that described for mitochondrial proteins in retinal neurons.[35,36] The steady-state levels of *Ngb* mRNA, as determined by qRT-PCR, were significantly higher in retinas from eyes that received early or late treatment than in retinas from untreated eyes; the increases were 3.4- and 3.6-fold, respectively (Figure S5C). Next, we used western blot analysis to evaluate the protein abundance in retinas from treated eyes of mice that received early treatment and in retinas from the contralateral untreated eyes (all mice were euthanized at 1 year of age). The NGB level increased 2-fold in retinas from treated eyes, as compared to retinas from untreated eyes, whereas no change was evident in the steady-state levels of the NDUFA9 and ATP synthase α proteins (Figures S5D and S5E). Hence, administering AAV2/2-*NGB* to DBA/2J eyes resulted in increased levels of both the *Ngb* transcript and the protein in the eyes up to 10 months after they underwent gene therapy.

Impact of AAV2/2-*NGB* Administration on Retinal Ganglion Cell Integrity and Gliosis

To evaluate whether *Ngb* overexpression could prevent RGC loss and the active growth of Müller-cell processes, we performed immunohistochemical staining for BRN3A and GFAP on retinal sections from DBA/2J mice that received early or late treatment and were euthanized at the age of 12 months. GFAP reactivity was less prominent in treated retinas than in untreated ones, regardless of when the treatment was carried out (Figures 7A and 7B). Indeed, the GFAP intensities in retinas subjected to early or late treatment were, respectively, 34.4% and 42% of that measured in 12-month-old untreated mice, suggesting a diminution of glial cell activation due to the presence of high levels of NGB (Figure 7D). Moreover, there were more BRN3A-positive cells in the retinas of the treated eyes of mice that received early treatment than in the retinas of untreated eyes. Conversely, the retinas of mice that received late treatment contained very few BRN3A-positive cells (Figure 7B). An estimate of the RGC numbers confirmed these observations: early treatment resulted in significant protection against RGC loss, with the number of RGCs in treated eyes being 82.4% of that in 2-month-old mice and 2.6 times more than that in age-matched untreated eyes. In contrast, in retinas from mice that received late treatment, the RGC count was 34.2% of that in the retinas of 2-month-old mice, and the extent of neuronal loss was very similar to that in the retinas of untreated 1-year-old mice ($p = 0.71$) (Figure 7C).

Morphologic Changes of Retinal Ganglion Cells after AAV2/2-*NGB* Treatment

To determine whether the increased accumulation of NGB in transduced cells could lead to structural changes in neurons, retinas mounted with the vitreal side (corresponding to the GCL)

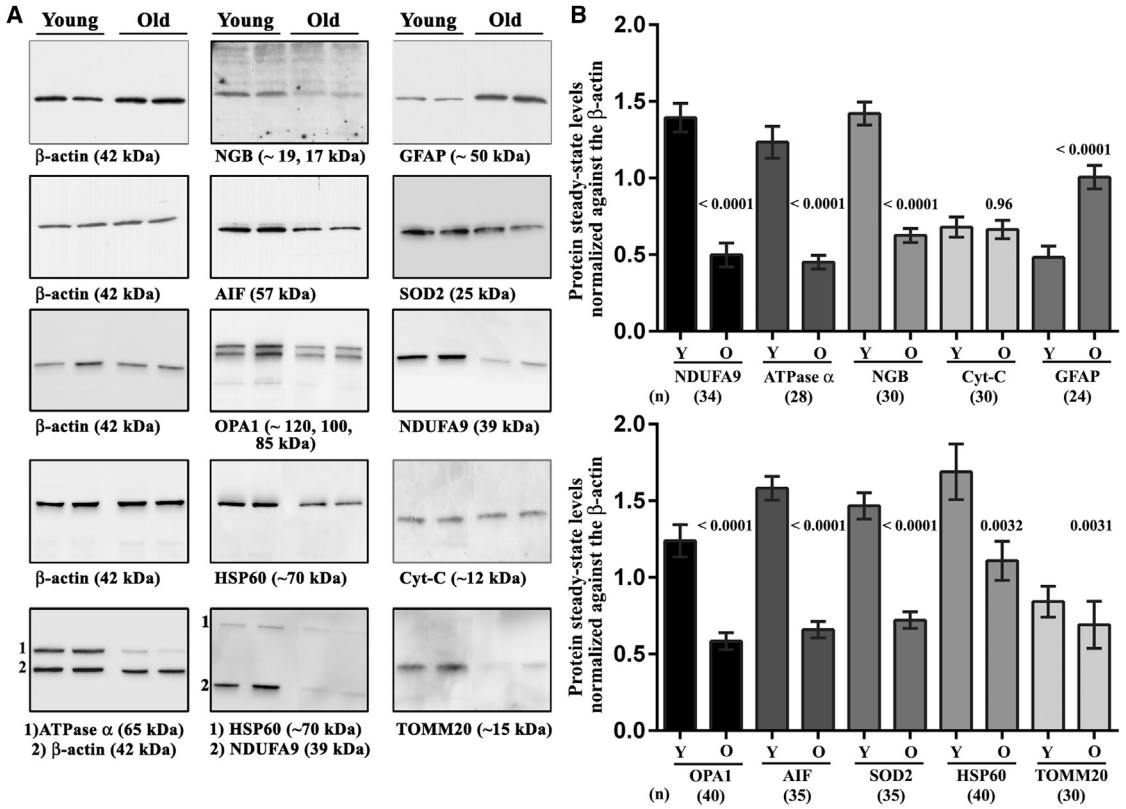

Figure 5. Mitochondrial Protein Abundance in Retinas from Young and Old DBA/2J Mice

(A) Western blots were performed with protein extracts from mice aged 2 months (the young group, Y) or 12 months (the old group, O), using various antibodies against mitochondrial proteins. A total of 17 individual retinas were evaluated for each group. The signals obtained with the antibody against β-actin (the loading control) and with two other antibodies against mitochondrial proteins are shown for five independent membranes. With the antibody against NGB, the strongest signal was detected at 17 kDa, and additional faint signals were often detected at approximately 19, 21, 25, and 34 kDa. We had previously observed the 19-kDa and 21-kDa proteins in rodent retinas.[18,20] The other signals corresponding to higher apparent molecular masses may indicate post-translational modifications such as phosphorylation[70] or dimerization of the protein.[71] The bottom row shows a membrane that was incubated with antibodies against two proteins simultaneously (1 and 2). (B) Bar charts showing the means ± SEMs calculated from separate immunoblots after they were scanned and their signals quantified with the Quantity One software. The relative levels of mitochondrial proteins were normalized against β-actin signals. For each protein, p values were calculated as the difference between the signals obtained in young and old DBA/2J mice. The number of individual signals for independent retinas used for the calculations is shown for each protein below the corresponding bars.

uppermost were double labeled with antibodies against BRN3A and β3-tubulin, a specific marker for dendrites and axons of RGCs and amacrine cells. Retinas from the treated eyes of mice that received early (n = 7) or late (n = 10) treatment were compared with retinas from untreated mice aged 2 months (n = 7) or 12 months (n = 8). The periphery of the retina displays more clearly the somas, axons, and dendrites of isolated neurons within the GCL, enabling a better evaluation of their morphology by confocal microscopy (Figures 8 and 9). Few RGCs were observed in the retina from the 12-month-old untreated mouse or in the treated retina collected from the mouse that received late treatment, whereas transduced retinas from mice subjected to early treatment displayed a density of RGCs comparable to that found in the retina from the young mouse. The overall morphology of the RGCs and their connections appeared to be preserved in transduced retinas independently of when the treatment was performed. This point is illustrated in the β3-tubulin panels of Figures 8 and 9, in which some BRN3A-positive cells (identified by white arrowheads) have short/few dendrites and other BRN3A-positive cells (identified by red arrowheads) have longer dendrites.

In retinas from mice subjected to early treatment and euthanized at the age of 12 months, the structural hallmarks of RGCs; i.e., their density, their branching, and the extent of their dendrites, were comparable to those of RGCs of young mice. However, in the retinas from the contralateral untreated eyes, not only was the number of RGC somas diminished, but the surviving cells exhibited few connections with the neighboring neurons (Figure 8). When we compared retinas from two mice that received late treatment and retinas from two age-matched untreated mice, it was clear that neurons in retinas of treated mice had better-preserved morphology with respect to their dendritic profiles (Figure 9). Hence, AAV2/2-*NGB* administration protects against

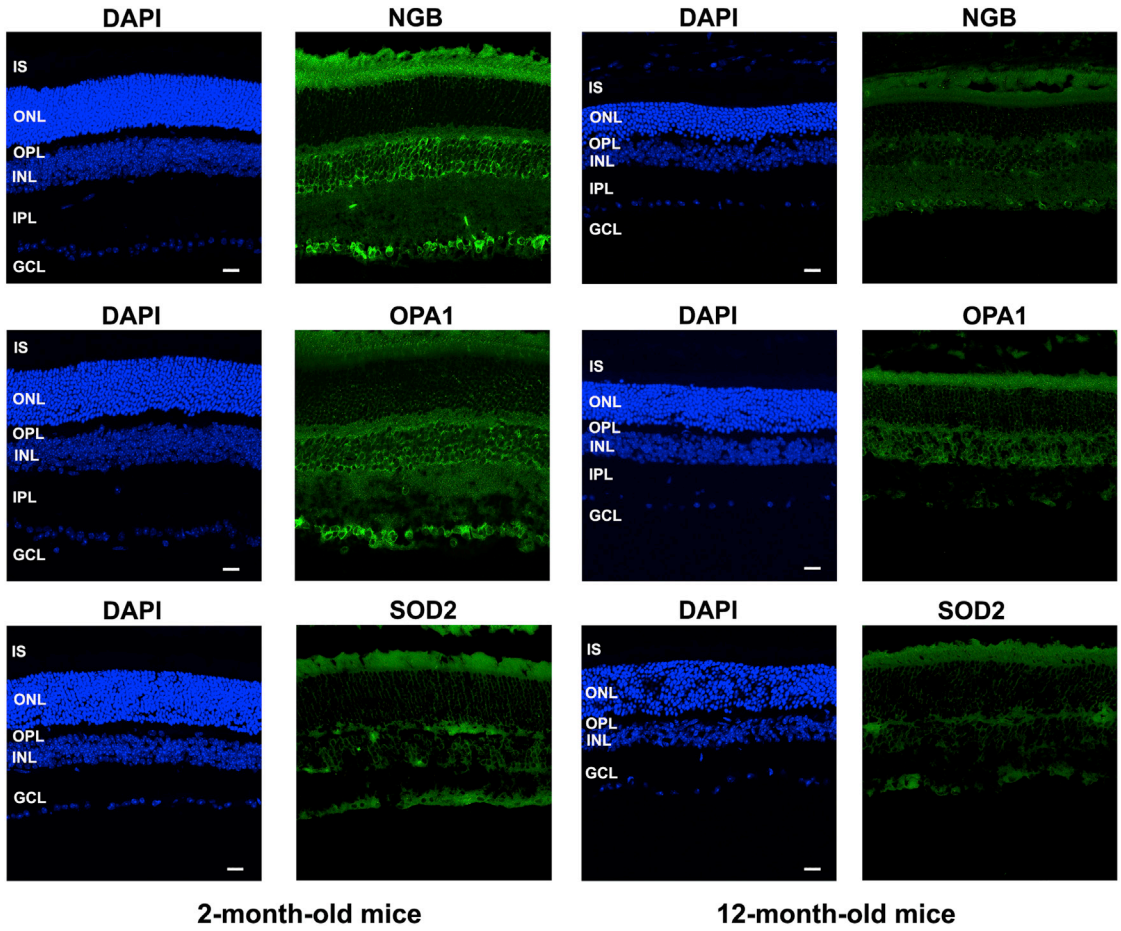

Figure 6. Mitochondrial Protein Abundance and Distribution in Different Retinal Cell Layers

The abundance and cellular distribution of the mitochondrial proteins NGB, OPA1, and SOD2 was examined by indirect immunofluorescence in retinal sections from 2- and 12-month-old DBA/2J mice (approximately six mice were evaluated for each age group). Nuclei were stained with DAPI (blue). The scale bars represent 20 μm. Abbreviations: ONL, outer nuclear layer; IS, inner segments of photoreceptors; INL, inner nuclear layer; GCL, ganglion cell layer; OPL, outer plexiform layer; IPL, inner plexiform layer.

neuronal death and is able to preserve the structural organization of the surviving neurons.

Consequences of Neuroglobin Overexpression for ON Morphology and Function

We estimated the number of NF200-positive spots in ON sections from the treated eyes of mice that received early or late treatment and in ONs from age-matched untreated animals (Figures 10A and 10B). There was no significant loss of nerve fibers in the ONs of the treated eyes of mice that received early treatment when compared to the ONs of young animals ($p = 0.51$), whereas ONs from mice that received late treatment exhibited a 78% reduction in the number of nerve fibers when compared to the ONs of young mice; this decrease was similar to that seen in untreated age-matched animals ($p = 0.85$) and confirmed that treatment at the later age was unable to prevent RGC degeneration. We also performed immunohistochemical staining of sections of ONs with antibodies against GFAP, IBA1, and vimentin (Figures 10B and 10D); remarkably, ONs from treated animals showed a noticeable diminution in the intensity of the fluorescent signals obtained with these antibodies. Figure 10D shows the mean fluorescence for the three antibodies in ONs of treated eyes, normalized against the results obtained with 12-month-old untreated mice. Hence, the microglial and astrocyte activation that accompanies glaucoma progression may be reduced as a result of the increased amount of NGB in RGCs.

To establish whether morphologic changes in retinas and ONs can result in improved energy metabolism, we assessed the respiratory chain function in the ONs of the treated eyes of mice that underwent AAV2/2-*NGB* administration at 2 or 8 months of age (Figure 11A). The CV activity did not change in any of the groups evaluated, as demonstrated in untreated DBA/2J mice at various ages (Figure 4). The specific activity of CI, expressed as nanomoles of oxidized "NADH/min/mg", in ONs of treated eyes of mice that received early or late treatment (9.22 ± 0.49 and 7.83 ± 0.46, respectively) corresponded to 76.7% and 65%, respectively, of that measured in the

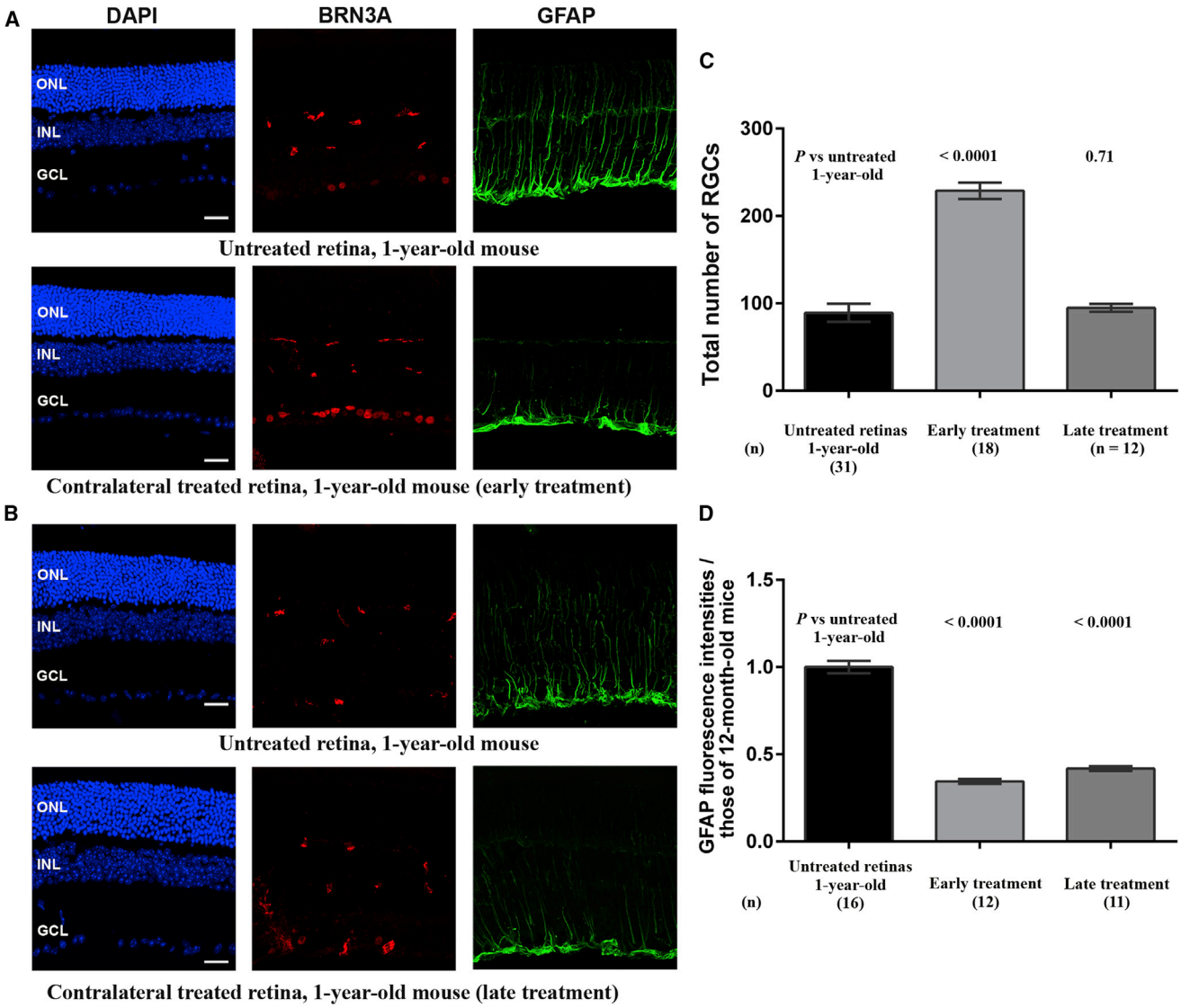

Figure 7. Effects of AAV2/2-*NGB* Treatment on DBA/2J Retinas

(A) Immunofluorescence analysis of retinal sections from a 1-year-old mouse in which one eye underwent intravitreal injection of AAV2/2-*NGB* at 2 months of age (early treatment) and the contralateral eye remained untreated. (B) Immunofluorescence analysis of retinal sections from a 1-year-old mouse in which one eye underwent intravitreal injection of AAV2/2-*NGB* at 8 months of age (late treatment) and the contralateral eye remained untreated. For (A) and (B), confocal images illustrate immunolabeling for BRN3A (red) and GFAP (green). The nuclei were stained with DAPI (blue). The scale bars represent 20 μm. Abbreviations: ONL, outer nuclear layer; INL, inner nuclear layer; GCL, ganglion cell layer. (C) The overall number of RGCs was estimated by counting BRN3A-positive cells in retinas from the treated eyes of DBA/2J mice that underwent intravitreal injection of AAV2/2-*NGB* at 2 months (early treatment) or 8 months (late treatment) of age; all of the mice were euthanized at 1 year of age. The values obtained for treated retinas were compared to those obtained for untreated retinas from 1-year-old mice. The bar chart illustrates the mean numbers of RGCs ± SEMs; the number of mice evaluated in each group is shown in brackets. p values in treated retinas were calculated with respect to RGC values in untreated retinas from 1-year-old mice. (D) The bar chart illustrates the normalized values of the fluorescence intensity for GFAP labeling in entire retinal sections. The values were normalized against the mean fluorescence in retinas from 12-month-old mice. The number of retinal sections from independent mice evaluated with ImageJ is indicated below each bar. The values were plotted using GraphPad Prism 6 as means ± SEMs.

ONs of untreated 2-month-old mice (12.02 ± 0.86) (Figure 4). Hence, ONs of treated eyes of mice that received early or late treatment exhibited, respectively, a 2-fold or 1.7-fold increase in CI activity when compared to ONs of age-matched untreated mice (4.62 ± 0.3). The differences in CI activity between the treated and untreated groups were significant ($p < 0.0001$), regardless of when gene therapy was performed (Figure 11A). Determining the CI/CV ratio increased the robustness of the calculated CI activity in ONs as a consequence of *Ngb* overexpression: increases in activity of 78% and 50% were observed in ONs of treated eyes of mice that received early and late

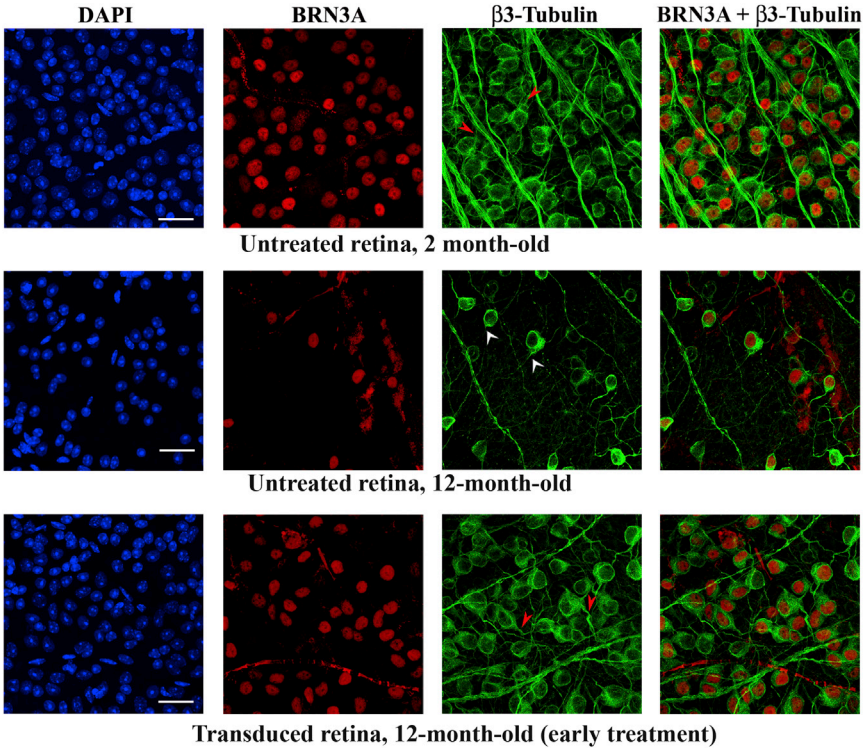

Figure 8. Morphology of Neurons in the Ganglion Cell Layer after Early Treatment with AAV2/2-*NGB*

Flat-mounted retina preparations (vitreal side up, with the GCL visible) were subjected to immunohistochemical staining with antibodies against BRN3A (red) and β3-tubulin (green). The results shown were obtained with three retinas: one isolated from a 2-month-old untreated mouse and two from a 12-month-old mouse subjected to AAV2/2-*NGB* administration at the age of 2 months (early treatment) and euthanized 10 months later. The observations were performed with a confocal microscope and regions from the periphery are illustrated. A composite image for BRN3A and β3-tubulin labeling is shown at the right. The nuclei were stained with DAPI (blue). The scale bars represent 25 μm. In the β3-tubulin panel, some BRN3A-positive cells are highlighted: white arrowheads indicate cells displaying short or few dendrites (untreated retina), and red arrowheads indicate cells with long dendrites (transduced retinas).

treatment, respectively, when compared with ONs of age-matched untreated mice ($p < 0.0001$).

Next, we evaluated the activities of CII + CIII, CIII, and CIV. Based on the samples tested, treatment at 2 or 8 months of age was significantly beneficial in all cases when the results were compared with those obtained in 12-month-old untreated mice (Figure 11B). For CII + CIII activity, we observed increases of 52.8% and 53.0% in ONs of treated eyes of early and late-treated animals, respectively, as compared to the activity in age-matched untreated controls ($p < 0.0001$ and $p = 0.008$ for early and late treatment, respectively). For CIII activity, the increases were 67.4% and 53.8% for early and late treatment, respectively ($p < 0.0001$ and $p = 0.0022$, respectively). For CIV activity, the increases in ONs of treated eyes of mice that received early or late treatment were 66.9% and 64.8%, respectively, relative to that in age-matched untreated animals ($p < 0.0001$). Thus, *Ngb* overexpression compensated for respiratory chain deficiency in ONs, which could lead to improved RGC functionality.

Preserved Retinal Ganglion Cells in AAV2/2-*NGB*-Treated Eyes Elicited Increased Neuronal Activity in the Visual Cortex

We recorded flash visual evoked potentials (F-VEPs) in treated DBA/2J mice to assess whether the preserved morphologic hallmarks of RGCs, along with the improved respiratory chain activity in ONs, could enhance visual function. F-VEPs are used to monitor communication from the RGC soma through the axon to the visual cortex by recording electrical potentials from the brain after visual stimulation.[37] F-VEPs in young DBA/2J mice produce robust and reproducible signals, but the signals are severely diminished in old animals.[38,39] Four groups were evaluated: (1) 19 untreated 2-month-old DBA/2J mice; (2) 21 untreated 1-year-old DBA/2J mice; (3) 27 1-year-old DBA/2J mice that received early treatment; and (4) 18 1-year-old DBA/2J mice that received late treatment. Light-adapted electroretinograms (ERGs) were first obtained to measure the functionality of the photoreceptor visual pathways of the mice.[40] Recordings made under these conditions essentially consist of a fast positive b-wave that reflects the cone response to light stimulation (Figure S6, left; Table S1). In some 1-year-old DBA/2J mice, we observed a decrease in the b-wave amplitude that might have been associated with iris or corneal injury. Mice in which b-wave amplitudes reached only 25% or less of the values measured in untreated 2-month-old mice and which exhibited severe corneal pathology were excluded from subsequent analyses. The most consistent components of F-VEPs are a negative N1 and a positive P1 peak, as shown in Figure 11C (left panel). We found no differences in the peak latencies or peak-to-peak amplitudes when the responses for right and left cortices were compared, probably because at the optic chiasm of mice, more than 95% of the fibers from the nasal part of the retina decussate and join the uncrossed temporal fibers of the opposite nerve to form the optic tracts.[41] Thus, responses from right and left visual cortices were averaged, because their signals originate from fibers of each eye. The latencies of the N1 and P1 peaks, along with the P1-wave amplitudes, were similar in all mice evaluated (Table S1). Conversely, in the 12-month-old untreated DBA/2J mice, there was a decline of 42.3% in the calculated N1-wave amplitudes, as compared to those in young mice ($p = 0.0003$). AAV2/2-*NGB* administration in mice aged 2 or 8 months undeniably led to a significant enhancement of

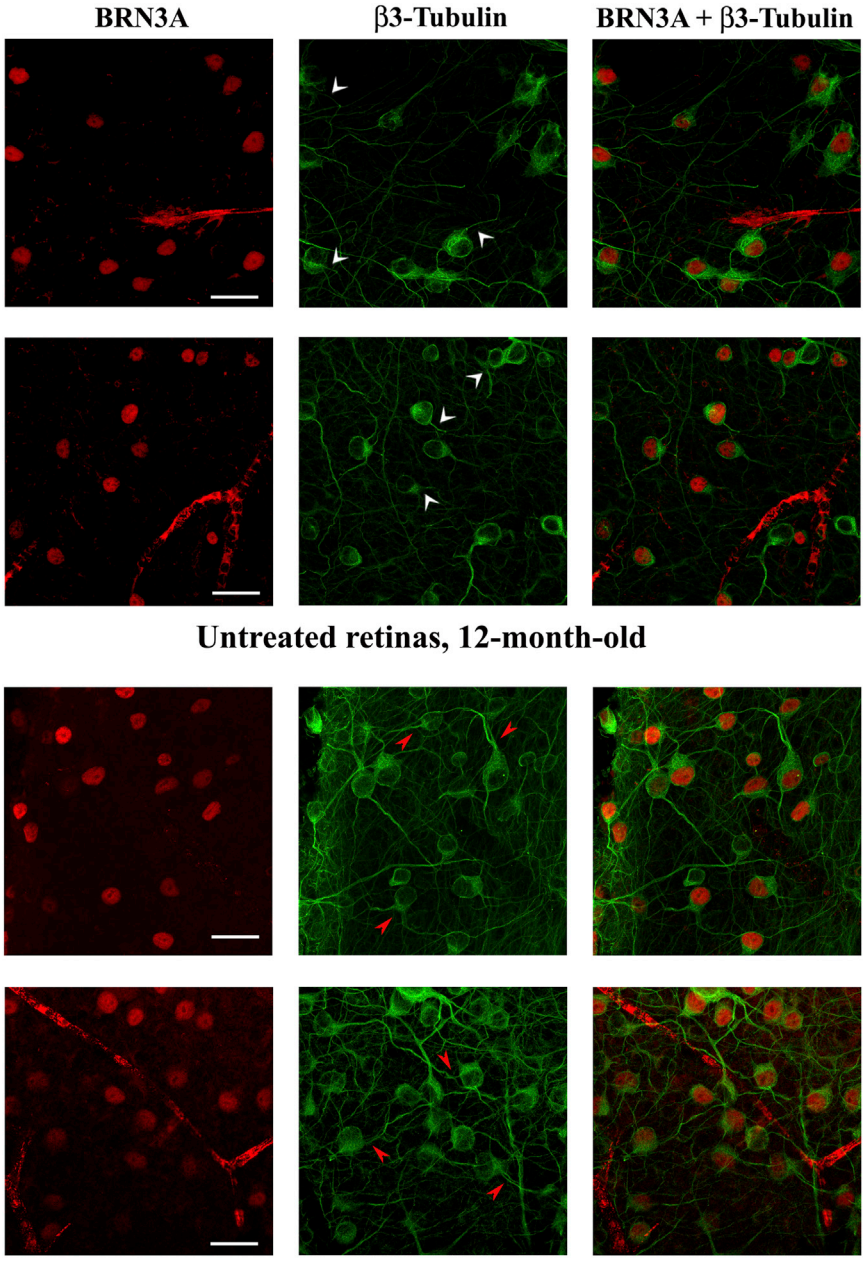

Figure 9. Morphology of Neurons in the Ganglion Cell Layer after Late Treatment with AAV2/2-*NGB*

Flat-mounted retinas from two untreated 12-month-old mice were compared to retinas from two mice that underwent intravitreal injection of AAV2/2-*NGB* in each of their eyes at 8 months of age (late treatment). The confocal images shown correspond to the peripheral region of the retinas. A composite image for BRN3A and β3-tubulin labeling is shown at the right. The nuclei were stained with DAPI (blue). The scale bars represent 25 μm. In the β3-tubulin panel, some BRN3A-positive cells are highlighted: white arrowheads indicate cells displaying short dendrites (untreated retinas from old mice), and red arrowheads indicate cells with long dendrites (transduced retinas).

N1-wave amplitudes, which reached 188% or 189%, respectively, of those in 1-year-old untreated mice (Figure 11C, right panel). Furthermore, N1-wave amplitudes in treated mice, regardless of when the treatment was performed, were not significantly different to the amplitudes measured in 2-month-old mice ($p = 0.93$ and 0.33 for mice that received early and late treatment, respectively). Thus, *Ngb* overexpression resulted in functional recovery, and RGCs became capable of providing high electrical inputs to the brain, which eventually induced enhanced visual cortex activity.

DISCUSSION

Glaucoma is characterized by a complex and progressive pattern of molecular changes that ultimately leads to blindness, although there are substantial differences among patients. Because elevated IOP is a major risk factor for glaucoma, the current treatment strategies are aimed at reducing IOP, but there is no effective cure.[42] The fundamental cause of glaucoma is the degeneration of RGC somas and axons,[9] as occurs in hereditary optic neuropathies.[13] RGCs are susceptible to mitochondrial dysfunction or disturbances of the mitochondrial network dynamics.[9] The nerve-fiber layer within the retina requires high energy for electrical conduction in the unmyelinated axons within the prelaminar and laminar parts of the ON; consequently, these fibers have a high density of mitochondria.[43]

Our objective was to determine whether mitochondrial impairment could be directly involved in glaucoma pathogenesis. The hallmarks of eye pathology in DBA/2J mice were described many years ago;[21,44,45] elevated IOP due to the release of iris pigment clumps into the anterior chamber of the eye is responsible for RGC loss and optic neuropathy.[21] We thoroughly characterized these mice and identified several phenotypic hallmarks: (1) iris fragmentation was observed in 4-month-old mice; (2) increased IOP was detected in 7-month-old mice, with the levels remaining high until the age of 12 months and diminishing thereafter; (3) RGC loss was evident in 10-month-old mice, whose retinas had less than 30% of the number of RGCs seen in young DBA/2J mice; (4) in retinas of 8-month-old DBA/2J mice, Müller cells responded to RGC injury by undergoing hypertrophy, with targeted cellular migration across the plexiform layers; (5) the activation of astrocytes and glial cells in ONs was obvious several

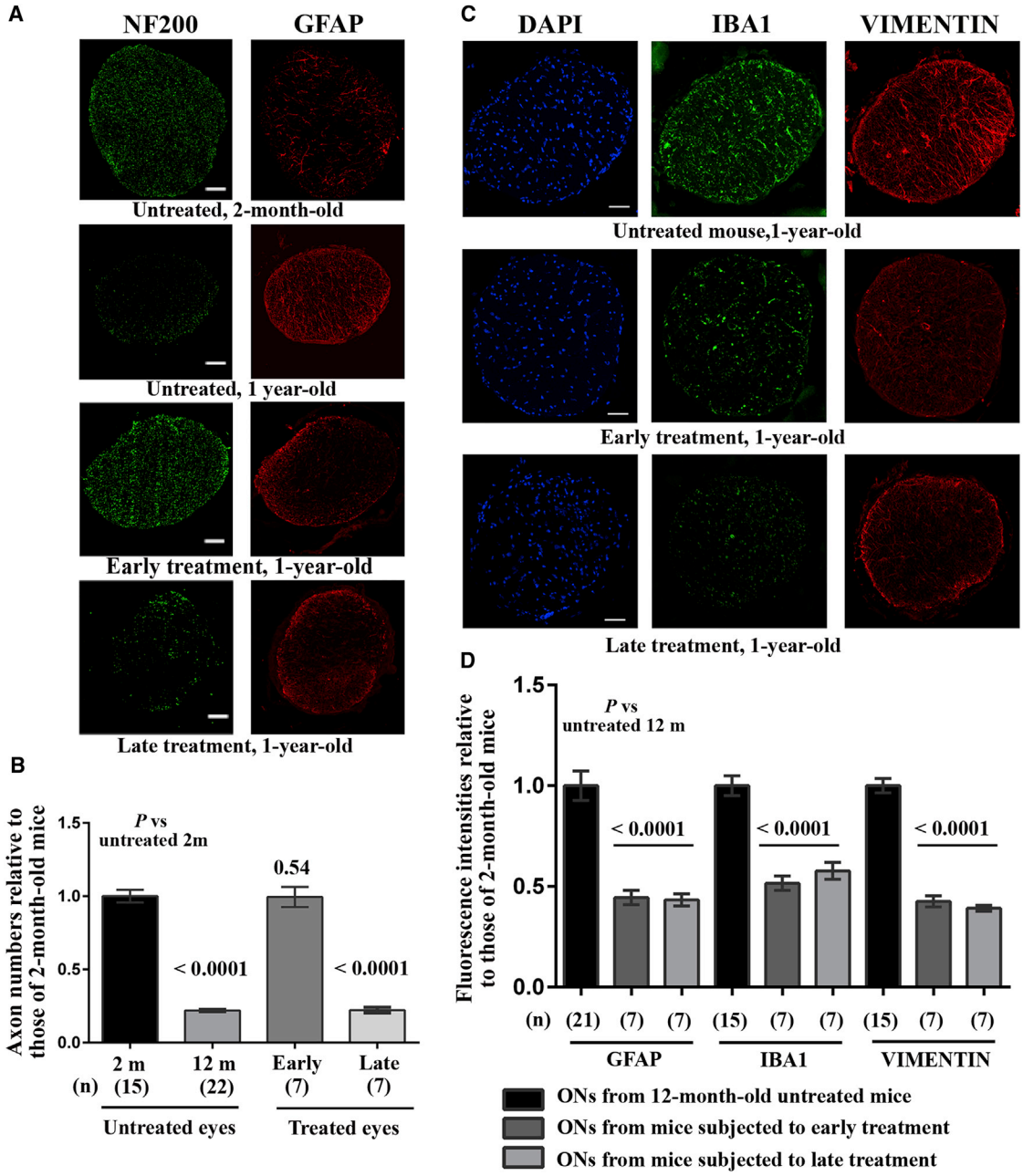

Figure 10. Optic Nerve Morphology in Retinas Transduced with AAV/2-*NGB*

(A) Proximal ON transverse sections were subjected to immunohistochemical staining with antibodies against NF200 (green) and GFAP (red). Results obtained from four mice are shown. From top to bottom: untreated 2-month-old mouse; untreated 1-year-old mouse; 1-year-old mouse subjected to early treatment; and 1-year-old mouse subjected to late treatment. The scale bar represents 50 μm. (B) Bar chart of estimated axon numbers (NF200-positive spots) for mice in the same groups as in (A); the number of mice evaluated in each group is shown in brackets below each bar (n). p values were calculated with respect to the number of fibers in untreated 2-month-old DBA/2J mice. (C) Results of immunohistochemical staining with antibodies against IBA1 (green) and vimentin (red) of ON sections from three 12-month-old mice. From top to bottom: untreated mouse; mouse treated at 2 months of age (early treatment); and mouse treated at 8 months of age (late treatment). The nuclei were stained with DAPI (blue). The scale bar represents 50 μm. (D) Normalized values (against the mean fluorescence in 12-month-old mice) for GFAP, IBA1, and vimentin labeling for the number of ON sections indicated beneath each bar (n). The values were plotted using GraphPad Prism 6 as means ± SEMs.

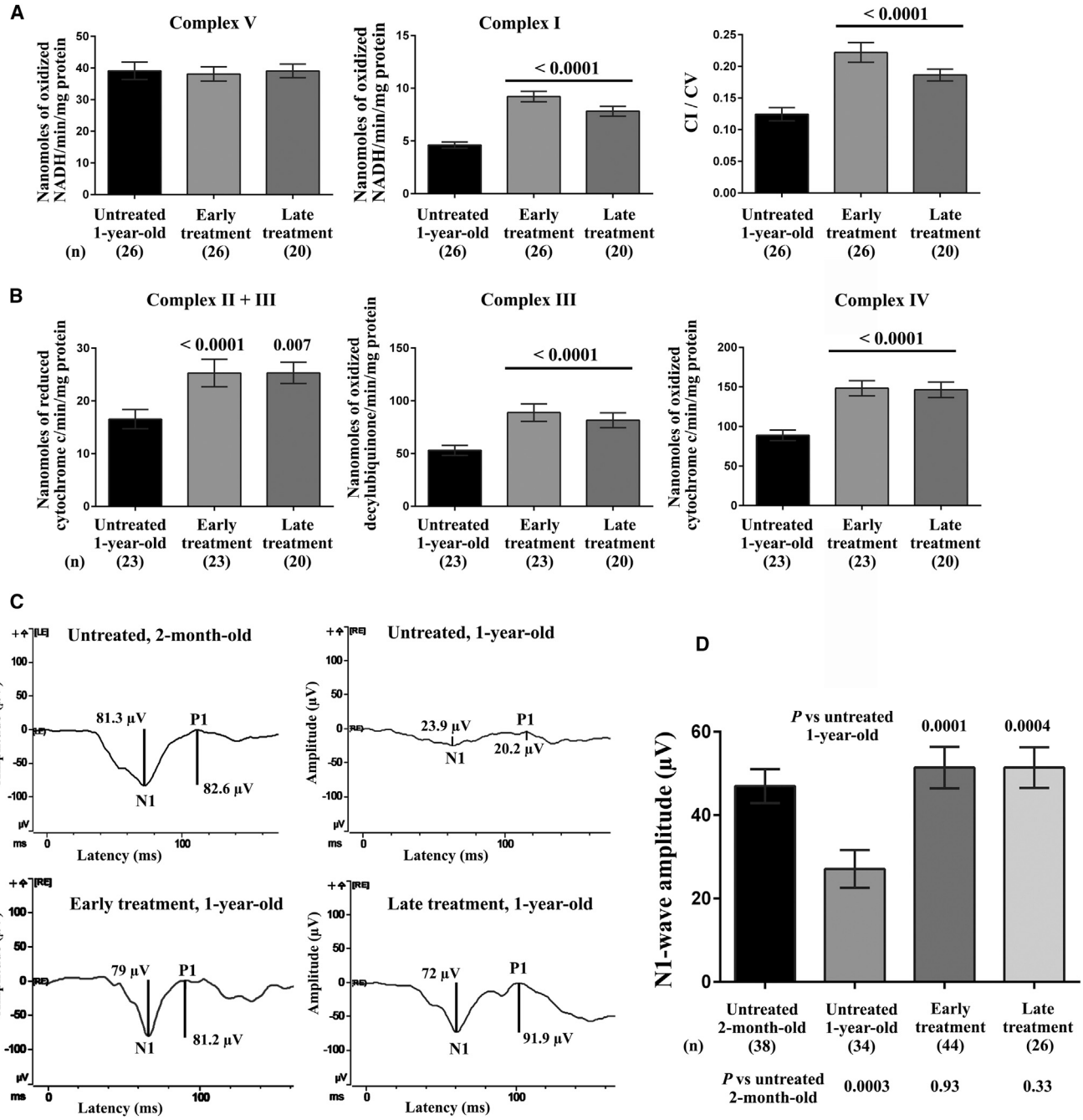

Figure 11. Effect of *NGB* Overexpression on Respiratory Chain Activity in Optic Nerves and on Visual Cortex Activity

The enzymatic activities of complexes I, II + III, III, IV, and V were measured in the following samples from 12-month-old mice: (1) 26 ONs from the treated eyes of mice that underwent intravitreal injection of AAV2/2-*NGB* at 2 months of age (early treatment); (2) 26 ONs from the untreated contralateral eyes of those same mice; and (3) 20 ONs from eyes that underwent intravitreal injection of AAV2/2-*NGB* at 8 months of age (late treatment). (A) The values shown in each bar chart represent the mean ± SEM of triplicates for CI and CV; the CI/CV ratio is also shown. (B) The values shown in each bar chart represent the mean ± SEM of duplicates for CII + CIII, CIII, and CIV for the samples evaluated. p values were calculated with respect to each activity as assessed in untreated 12-month-old mice. (C) Plots of F-VEP recordings with the N1 and P1 waveforms from two untreated DBA/2J mice aged 2 months and 1 year, one 1-year-old DBA/2J mouse in which one eye received early treatment, and one 1-year-old DBA/2J mouse in which both eyes received late treatment. (D) Bar chart of the peak amplitudes of the N1 waves for the four groups of mice evaluated. The data represent the means ± SEMs. p values were calculated with respect to data recorded in 12-month-old untreated mice; the number of individual responses for each group is indicated in brackets.

months before the disappearance of RGC axons, as previously described;[46] and (6) axonal degeneration was initiated in 8-month-old animals, with the loss of 33.3% of the nerve fibers present in healthy mice, thus preceding RGC soma disappearance by 2 months.

For the first time, we have demonstrated a consistent reduction in the enzymatic activities of respiratory chain complexes CI, CII + CIII, CIII, and CIV in retinas and ONs, with the decreases largely preceding the onset of neuronal loss. Energy supply defects may exacerbate the neurodegenerative process and certainly play a key role in optic neuropathy and vision loss. Moreover, retinas from DBA/2J mice aged 12 to 14 months exhibited a significant reduction in the steady-state levels of mitochondrial proteins involved in energetic metabolism, organelle dynamics, or antioxidant defenses. Proteomic studies investigating human retina samples from glaucomatous or ocular hypertensive patients established that an array of mitochondrial proteins displayed significant level reductions.[47,48] Consequently, insufficiency in the energy supply could initiate defects in electrical conduction and axonal transport, thereby leading to neuronal cell loss and, ultimately, glaucoma. Our data on the impairment of energy metabolism and the diminution of some mitochondrial protein amounts in DBA/2J mice support the notion that generalized organelle dysfunction could be a key player in the course of glaucomatous neurodegeneration. Hence, it is feasible to attempt therapeutic targeting of RGC mitochondria to preserve their function, with the aim of prolonging neuronal survival.

We chose to evaluate the effect of enhancing *Ngb* expression in RGCs via a single intravitreal injection of an AAV2/2 vector, because NGB levels were almost halved in the retinas of 1-year-old DBA/2J mice, as compared to those of 2-month-old mice. Since its identification in 2000,[14] NGB has been implicated in neuronal protection from hypoxia and oxidative stress.[49] In rodent or human retinas, NGB is differentially distributed in the retinal cell layers, with an increased abundance in the GCL and especially in RGCs,[18,20,50–52] as we showed in retinas from DBA/2J mice. A recent article reviewed the available data on the neuroprotective role of NGB in a range of pathologic conditions.[53] The possible mechanism of action that leads to the beneficial effect of NGB on nerve-cell survival appears to be linked to mitochondrial function by (1) the preservation of the ATP synthesis rate, ROS homeostasis, and mitochondrial membrane potential and (2) the modulation of death signaling via the shutdown of the apoptotic cascade.[53] For instance, the human NGB protein can efficiently scavenge a variety of ROS (superoxide anions, hydrogen peroxide, and hydroxyl radicals)[15] and also reactive nitrogen species (RNS), such as nitric oxide.[54] As for how NGB modulates the apoptotic process, it is envisaged that it depends on interactions with two mitochondrial proteins: the voltage-dependent anion channel (VDAC) and Cyt-C, a component of the respiratory chain. Binding between VDAC and NGB can modify the permeability of the outer membrane,[55] and because NGB is able to reduce Cyt-C, its leakage from damaged mitochondria and the subsequent caspase 9 activation could be impeded.[56,57] Furthermore, a recent study of mouse cortical neurons in culture demonstrated an interaction between NGB and Cyc1, a subunit of CIII. Within this complex, electrons are sequentially transferred from ubiquinol to Cyc1 and Cyt-C, and NGB could interfere in this transfer between Cyc1 and Cyt-C.[58] Interestingly, our experiments showed that *NGB* overexpression leads to increased enzymatic activity of CI and CIII. Hence, the impediment of noxious accumulation of ROS or RNS in the mitochondria and the protein-protein binding and intermolecular electron exchanges between Cyt-C/Cyc1 and NGB could ultimately lead to better performance of respiratory chain enzymes in ONs from DBA/2J eyes treated with AAV2/2-*NGB*. In 2014, we demonstrated that the retinas of Harlequin mice exhibited decreased steady-state levels of NGB. These mice display optic neuropathy due to a profound respiratory chain impairment,[19,59] which was efficiently prevented by injecting AAV2/2-*NGB* into the vitreous humor of young mice.[20] In this study, we confirmed the ability of NGB to sustain mitochondrial function; indeed, increased *Ngb* expression in the RGCs of 2- and 8-month-old DBA/2J mice resulted in significant protection of respiratory chain function in the ONs. These data highlight the fact that, regardless of the molecular mechanism involved in mitochondrial dysfunction, NGB efficiently protects against a failure in energy metabolism. The administration of AAV2/2-*NGB* to 2-month-old mice prevented RGC loss and nerve-fiber disappearance. In contrast, performing the same treatment in 8-month-old mice failed to prevent neuronal loss; however, the enhanced energy metabolism of the surviving RGCs led to the preservation of visual cortex activity.

We measured electrophysiologic signals corresponding to visual cortex activity by recording F-VEPs. The N1 and P1 peaks are generated by retino-geniculate fibers, which represent the main connection between the ON and the occipital cortex. If RGCs are functionally compromised, the sensory input after light stimulation cannot reach the visual cortex; therefore, the F-VEP is considered a quantitative index of visual function.[37] We demonstrated that 12-month-old DBA/2J mice displayed a 42% reduction in the N1-wave amplitude relative to the values observed in 2-month-old DBA/2J mice, which is consistent with the extensive RGC injury. AAV2/2-*NGB* administration led to an effective restoration of RGC functionality, because no significant difference was found between the N1-wave amplitudes in young mice and those in their 1-year-old counterparts, which accumulated increased amounts of NGB in their RGCs as a result of undergoing gene therapy at the age of 2 or 8 months. In the latter animals, the RGC number was low at the time of euthanasia; nevertheless, respiratory chain function in the ONs was preserved, as were the cortical responses to light stimulation. Thus, the surviving RGCs elicited improved visual cortex activity, for which there are several possible explanations: (1) there are more intense action potentials from the residual RGCs; (2) RGC axons constitute more synapses in their target area (the superior colliculus [SC]) and are thus able to connect more neurons; or (3) SC neurons can generate additional axonal collaterals and sprouts, with positive consequences for visual function. These situations have been described in several models: in adult hamsters, single regenerated RGC axons efficiently contacted multiple SC neurons, and a limited number of RGCs with regenerated axons were able to drive a much larger number of neurons in the occipital cortex,

resulting in increased behavioral responses to light.[60] In a rodent model of glaucoma due to elevated IOP, at a late stage of the disease, compensatory functional changes were evident in the terminals of surviving cells, possibly as a result of plasticity, leading to increased synaptic transmission in the SC.[61,62] In a model of glaucoma induced by cauterizing the episcleral vein, changes were observed in the INL, such as newly formed synapses between RGCs and bipolar cells and the expansion of RGC dendrites.[63]

By carefully comparing flat-mounted retinas from *NGB*-treated and untreated 1-year-old mice, we observed distinct changes in RGC morphology, suggesting that neuronal remodeling and synaptic plasticity occurs inside the retina. This could explain, at least partially, the enhanced visual cortex activity in treated mice.

Because mitochondrial integrity, and especially organelle motility, is required to provide energy for synaptic signaling and plasticity,[64] we postulate that NGB, by virtue of its ability to protect the respiratory chain, is responsible for preventing RGC loss and axonopathy when administered to young DBA/2J mice. When the treatment was administered at an advanced stage of the disease, the surviving RGCs were able to deliver a consistent electrical input to the brain. Hence, *Ngb* overexpression, by preserving the RGC energy metabolism status, leads to functional synaptic transmission through the ON to the occipital cortex. Furthermore, the enhancement of the amount of NGB in RGCs results in the reduction of both microglial activation and astrocyte proliferation in ONs, and the attenuation of inflammatory responses could also improve the transmission of nerve impulses to the central visual system. In DBA/2J mice, damage to RGCs and their subsequent loss occur in progressive stages that are initiated by ocular hypertension and involve the whole visual pathway. Most of the 1-year-old DBA/2J mice studied here exhibited extensive RGC death and axonal degeneration (with losses of 67% and 78%, respectively, relative to the numbers in 2-month-old mice). AAV2/2-*NGB* is a single-stranded parvovirus; therefore, the number of transduced RGCs is expected to reach a maximum between 4 and 6 weeks after vector injection into the vitreous body, as a result of the delay required for the conversion of the single-stranded viral genomes to double-stranded DNA molecules and their subsequent transcription.[65] The aim of treating 8-month-old mice was not to induce cell survival, as the therapeutic window had already passed, but to mimic the clinical situation, in which patients develop severe visual impairment long after the disappearance of RGCs has begun. In this regard, NGB was able to halt the degeneration of the remaining RGC axons, thereby maintaining both their bioenergetics and the ability to transmit signals to the visual cortex.

In conclusion, we have demonstrated that respiratory chain activity in the retinas and ONs of DBA/2J mice is compromised several months before the onset of RGC loss. Furthermore, 1-year-old mice exhibiting glaucoma accumulated in their retinas low levels of several mitochondrial proteins that can further compromise organelle functionality. Therefore, the beneficial and sustained effect of NGB on RGC viability and functional integrity encourages its use as a powerful means of maintaining robust and long-lasting mitochondrial activity within neurons, with the aim of treating visual impairment in glaucomatous patients.

MATERIALS AND METHODS

Mice

Mice of the DBA/2J strain and the congenic C57BL/6J strain were obtained from Charles River Laboratories (L'Arbresle, France). There were 2-month-old DBA/2J mice that were used as "healthy" controls, as these mice do not develop glaucoma until they are 8 to 10 months of age. For some experiments, C57BL/6J mice were also evaluated as controls that did not exhibit visual function impairment with aging.[25,29] The mice were housed one to four per cage in a temperature-controlled environment, with a 12 hr light/dark cycle and free access to food and water, in a pathogen-free barrier facility. The studies were conducted in accordance with the official guidelines for the care and use of animals in research and were approved by the French Ministry of Agriculture and the Veterinarian Department of Paris (permit no. DF/DF_2010_PA1000298), the French Ministry of Research (approval no. 5575), and the ethics committees of the University of Paris 6 and INSERM (authorization no. 75-1710).

Intraocular Pressure Measurements

For noninvasive measurement of IOP, an Icare TONOLAB tonometer (Icare) was used. The assessment is based on a rebound method, which allows the IOP to be calculated accurately, rapidly, and without the need for local anesthetic. The instrument takes six individual measurements, each repeated three times, and presents the mean of 18 values as a single reading displayed in "mm Hg". DBA/2J and C57BL/6 mice were studied between the ages of 2 and 15 months; measurements were performed monthly on both eyes and were made during daylight.

In Vivo Confocal Microscopy Analysis

A laser-scanning in vivo confocal microscope (IVCM) (Heidelberg Retina Tomograph [HRT] II/Rostock Cornea Module [RCM]; Heidelberg Engineering) was used to examine the entire cornea, including the superficial epithelium (at zero depth), basal epithelium (at a depth of 8–15 μm), stroma (at a depth of 15–40 μm), and endothelium (at a depth of 65–80 μm).[66] We used the protocol to visualize the iris at depths ranging from 80 μm to 160 μm. Groups of four mice aged 2, 4, 8, or 12 months were each subjected twice to this analysis.

In Vivo Electrophysiology

Photopic ERGs and F-VEP responses were recorded simultaneously from electrodes placed on the cornea and overlaying the visual cortex, respectively. Photopic ERGs were assessed using two gold loop electrodes with light stimuli (10 cd.s/m^2) applied on a light background (20 cd/m^2) as previously described.[67] For F-VEPs, deep anesthesia was induced in the mice 7 days before the recording and maintained with 2% to 3% isoflurane (Axience and Abbott) administered through a face mask. Two stainless-steel screws (diameter, 0.9 mm and length, 2.4 mm) were implanted, using X and Y stereotaxic coordinates, into the right and left visual cortices and fixed in place with surgical glue.

Each electrode was positioned 2.7 mm posterior to the bregma and 2.5 mm lateral to the right or left lambda suture and penetrated the cortex to a depth of 1 mm. Platinum needles in the forehead and at the base of the tail served as reference and ground electrodes, respectively. On the day of electrophysiologic recording, mice were anesthetized with an intraperitoneal injection of a mixture of ketamine (100 mg/kg) and xylazine (10 mg/kg). Their body temperatures were maintained at 37°C to 38°C with a heating pad, and their pupils were dilated with a single dose of 1% tropicamide and 5% phenylephrine. Stimuli for the ERGs and F-VEP response recordings were generated and controlled by an Espion E2 system (Diagnosys). A single flash stimulus was delivered in a Ganzfeld dome. For photopic ERGs, each flash had a duration of 4 ms, and the signals were differentially amplified and digitized at a rate of 5 kHz with a band-pass filter (0–300 Hz). VEP responses were elicited by 100 flashes of white light (10 cd/mm^2 each), with a duration of 4 ms each and a frequency of 1 Hz, delivered with the flash photostimulator placed 15 to 20 cm from each eye with a band-pass filter (10–80 Hz). Photopic ERGs consist of a b-wave with positive polarity derived from the inner retina, which corresponds to the cone responses after light stimulation.[40] The mouse F-VEP is dominated by a negative polarity component (N1) that peaks at 50 to 80 ms after stimulus presentation. The implicit time of the N1 component was measured at the negative peak. The amplitude of the F-VEP was measured from the N1 negative peak to the ensuing positive peak (P1).[68]

The amplitude and timing of the ERG and VEP components were measured with the Espion software by placing a cursor at a subjectively determined turning point (the peak or trough) for each component of the individual recordings. There were two experimenters that performed the evaluations independently without knowing what treatment the mice had received.

In some 12-month-old DBA/2J mice, a decreased response in the ERG might be associated with iris or corneal injury impeding light stimulation of the inner retina. Hence, mice in which the ERG responses attained values that were only 25% or less of those measured in untreated 2-month-old mice and which exhibited severe corneal injury were excluded from subsequent analyses. Four mice in the untreated 12-month-old group and five mice in each of the treated groups were excluded on this basis.

Adeno-associated Viral Vector and Intravitreal Injections

The design of the AAV2/2-*NGB* vector was described previously.[20] Briefly, the recombinant pAAV-IRES-*hrGFP* vector (Agilent Technologies) contains the coding sequence (453 bp), 5′ UTR (279 bp), and 3′ UTR (895 bp) of the mouse *Ngb* gene. AAV vectors were produced by the INSERM UMR1089 research unit (Nantes, France). For intravitreal injections, DBA/2J mice were anesthetized with 2% to 3% isoflurane (Axience). The tip of a 33-gauge needle, mounted on a 10 μL Hamilton syringe (Hamilton Bonaduz), was advanced through the sclera and 2 μL of the AAV2/2-*NGB* vector suspension (2×10^9 vector genomes) was injected intravitreally into the superior area of the retina, avoiding structural disruption, bleeding, or lens injury. In terms of disease progression, two types of gene therapy were performed: "early treatment", in which the vector was administered to 55 2-month-old mice in one eye only, and "late treatment", in which the vector was administered to 18 8-month-old mice; in the latter group, 16 of the 18 mice received the vector in both eyes. All surviving mice were euthanized at 12 months of age. In the early treatment group, nine mice died from natural causes before reaching 12 months of age and were, therefore, excluded from subsequent studies.

Retinal and ON Histology

Mice under anesthesia were killed by cervical dislocation, whereupon their eyes were enucleated immediately and dissected. After the anterior segment and vitreous humor had been removed from each eye, the retinas and ONs were collected, fixed in 4% paraformaldehyde (PFA) at 4°C, then cryoprotected by overnight incubation in PBS containing 30% sucrose at 4°C. Retinas were embedded in optimum cutting temperature (OCT) medium (Neg 50; Richard-Allan Scientific) and frozen in liquid nitrogen. ONs were embedded in a solution of PBS + 7.5% type A gelatin from porcine skin (Sigma-Aldrich) and 10% sucrose and frozen in a 2-methyl-butane solution at −45°C. Sections of retinas and ONs were cut (at a thickness of 10 μm) on a cryostat (Microm HM 560; Thermo Scientific) at −20°C and mounted on Superfrost Plus slides. For the retinas, approximately 16 consecutive slides were obtained for each eye, half corresponding to the superior side.

For immunohistochemical analysis, retinal and ON sections were treated for 10 min with PBS + 0.1% Triton and then for 1 hr with a solution of 1% BSA, 0.1% Triton, 0.05% Tween 20, and 5% normal goat serum (Sigma-Aldrich) and incubated with the primary antibodies overnight at 4°C. Next day, the sections were washed in PBS (three times for 10 min each) and incubated with the appropriate secondary antibodies and DAPI (Sigma-Aldrich) for 2 hr at room temperature. Finally, the sections were washed three times with PBS, rinsed with sterile water, and mounted on glass slides. Flat-mounted retinas were obtained after enucleating eyes and removing the anterior segment and vitreous humor. Each retina was treated with 4% PFA at 4°C overnight. Next day, they were rinsed twice with PBS (15 min per wash) then permeabilized with PBS and 1% Triton X-100 for 10 min. They were then incubated in 3% BSA, 0.1% Triton X-100, and 0.05% Tween 20 for 2 hr at room temperature with gentle stirring. Primary antibodies were added at the appropriate concentrations to the same solution used for the saturation step and incubation was performed overnight at 4°C with gentle stirring. Next day, the retinas were washed twice with PBS (15 min per wash) at room temperature and incubated with secondary antibodies and DAPI for 2 hr at room temperature in the dark with gentle stirring. After this incubation, the retinas were rinsed twice with PBS (15 min per wash) and two incisions were made at each end under binocular magnification. The retinas were then carefully flattened and mounted on glass slides with the vitreal side, corresponding to the GCL, uppermost. The primary and secondary antibodies used for immunohistochemical staining are shown in Table S2.

Microscopic Observations and Analyses of Images

Fluorescence labeling was monitored with a confocal laser scanning microscope (Olympus FV1000 or Leica TCS SP8); images were acquired with Olympus FluoView or LAS X software. Retinal sections were also scanned with a NanoZoomer Digital Pathology (NDP) 2.0 HT scanner (Hamamatsu Photonics), using the Fluorescence Unit option (L11600-05) and the NanoZoomer's 3-CCD TDI camera. After whole retinal sections scanned with the NDP 2.0 HT scanner (Hamamatsu Photonics) had been reconstructed, the number of RGCs was estimated using the NDP analyze software. For each mouse, the number of cells that were positive for BRN3A was counted over the entire length of three or four retinal sections. Published data obtained from mice indicate that a high-density region for RGCs localizes to the superior retina as a horizontally oriented area extending nasotemporally, approximately 1 mm dorsal to the optic disk.[34] Thus, the sections counted corresponded to the superior retina at a depth of 400 to 600 μm from the ON. The same regions were chosen for evaluating the RGC number after gene therapy, because AAV2/2-*NGB* was administered to the superior side of the eye. Additionally, eye elongation related to IOP elevation has been described in DBA/2J mice; one study found that the axial length increased progressively after the age of 6 months and reached a "plateau" approximately 5 months later.[69] In our hands, the retinal length in reconstructed scanned images increased in mice aged 8 months or older relative to that seen in 2-month-old mice; no changes were observed after AAV2/2-*NGB* treatment (Table S3). Hence, for each mouse, we considered the average total number of RGCs in the retinal sections evaluated, regardless of their length. ImageJ software (National Institutes of Health) was used to create binary images by thresholding. The intensity of GFAP staining was estimated by measuring the mean fluorescence with the plot profile routine of ImageJ after reconstructing whole retinal sections with the NDP 2.0 HT scanner. There were three or four independent retinal sections that were evaluated for each mouse. In the ON sections, the number of RGC axons was deduced from the fluorescent spots revealed by the NF200 antibody. The total number of "particles"; i.e., the number of axons in each image, was automatically estimated for each mouse by analyzing three independent ON sections, as described previously.[20] The intensity of the labeling for vimentin, IBA1, and GFAP was also estimated in the ON sections by measuring the mean fluorescence, using the plot profile routine of ImageJ on three or four independent ON sections for each mouse assessed.

RNA Extraction and qRT-PCR Assay

Total RNA was extracted from retinas with an RNeasy Plus Mini Kit (QIAGEN). The RNA was treated with RNase-free DNase (QIAGEN) then cleaned with an RNeasy MinElute Cleanup Kit (QIAGEN). There was 1 μg of total RNA that was reverse transcribed using oligo-dT and SuperScript II reverse transcriptase (Life Technologies). qPCR reactions were performed using an ABI 7500 Fast Real-Time PCR System (Applied Biosystems) and the specific primers listed in Table S4, as described earlier.[20] Briefly, for each gene, the equivalents of 2 ng and 10 ng of cDNA were used as templates for qPCR reactions performed using Power SYBR Green PCR Master Mix (Applied Biosystems). Each biological sample was assayed in triplicate for each gene; the cycle threshold (Ct) values (the numbers of cycles required for the fluorescent signal to cross the background threshold) were obtained with the ABI 7500 software (v.2.0.4). To determine the relative mRNA amount for each gene studied, we used the comparative ΔΔCt method. The mitochondrial *Atp6* gene was used as the normalizing gene, because its mRNA steady-state levels remained almost unchanged in all the samples evaluated, as previously reported.[20]

Western Blot Analysis

For western blot analysis, retinas were isolated from 17 untreated 2-month-old mice (the young group) and 17 untreated mice aged 12 to 14 months (the old group). A further seven retinas were isolated from the treated eyes of mice that underwent AAV2/2-*NGB* administration at 2 months of age and were euthanized 10 months later, along with seven retinas from the untreated contralateral eyes of the same mice. The retinas were homogenized in 50 μL of 20 mM HEPES, 60 mM mannitol (pH 7.2), and protease inhibitor cocktail (Sigma-Aldrich) at 4°C with a 200 μL hand-driven glass-glass Potter-Elvehjem micro tissue grinder. Large cellular debris was concentrated by centrifugation (1,000 × *g* for 5 min at 4°C) and discarded. Then the amount of protein in the supernatants was quantified with Bradford assay reagent (Sigma-Aldrich) before western blotting was performed. After incubation at 95°C for 10 min, 15 or 30 μg of each sample was resolved by 12% SDS-PAGE and transferred to a PVDF membrane. The membranes were incubated with antibodies against mitochondrial proteins; immunoreactive bands were labeled with appropriate secondary antibodies coupled to horseradish peroxidase (Table S2) then detected with Pierce ECL Plus Western Blotting Substrate (Thermo Scientific). The apparent molecular mass of each protein was estimated by comparing each specific signal on the blots to the PageRuler Plus Prestained Protein Ladder (Thermo Scientific). Signals obtained were visualized with a G:BOX Chemi XX6 gel imaging system (Syngene Europe) and analyzed with Genesys software. Quantifications for different immunoblots were performed with Quantity One analysis software (Bio-Rad). We conducted these assays within the linear dynamic range of our detection method and corrected the intra- and interblot variability by loading two quantities of the protein extracts on the same gels/blots and including common samples in each independent experiment.[20] The signal obtained with the antibody against NGB generally revealed three bands, and we quantified the signal for the entire area encompassing these three bands. The incubation of the membranes with ReBlot Plus Strong Solution (Millipore) allowed three different antibodies to be used sequentially.

Tissue Homogenate Preparation and Respiratory Chain Enzymatic Assays

Samples from retinas and ONs were prepared by homogenization in 200 μL of extraction buffer (0.25 mM sucrose, 40 mM KCl, 2 mM EGTA, 1 mg/mL BSA, 20 mM Tris-HCl, pH 7.2) at 4°C with a 200 μL hand-driven glass-glass Potter-Elvehjem tissue grinder. The homogenates were subjected to low-speed centrifugation (1,000 × *g* for 8 min), and the supernatants were collected and frozen

at −80°C until use. Respiratory chain enzymatic activities were measured using a Cary 50 UV-Vis spectrophotometer (Agilent Technologies). We performed two spectrophotometric assays to measure sequentially the activity of the five respiratory chain complexes in a single retina or ON.[33] The first assay measured the activity of the rotenone-sensitive NADH decylubiquinone reductase (CI) and the ATP hydrolase activity of CV,[33] which is oligomycin sensitive. Each measurement was made in triplicate with 50 µL of the homogenate. In the second assay, the activity of cytochrome *c* oxidase (CIV) was measured by adding reduced Cyt-C and recording the oxidation rate. Next, the activity of succinate-cytochrome *c* reductase (CII + CIII) was initiated by adding succinate, which triggers the reduction of Cyt-C. Adding the SDH competitive inhibitor malonate fully inhibited the SDH-dependent activity. Finally, after metal chelation with EDTA, decylubiquinol was added to initiate the reduction of Cyt-C by CIII. CIII-specific activity was determined after adding antimycin, its specific inhibitor. The assay was performed in duplicate with 10 µL of each homogenate. After the protein had been quantified by the Bradford method, the values obtained from the assays were converted to specific activities for each complex, as presented in Table 1. All the chemicals used for the assays were of the highest grade available from Sigma-Aldrich.

Statistical Analysis

Statistical analyses were performed with GraphPad Prism 6.0 software, assuming a confidence interval of 95%. Generally, the observations within each group did not fit a normal distribution; therefore, nonparametric methods were applied to evaluate the significance. Data were compared using the Mann-Whitney *U* test for unpaired nonparametric significance. For mice that received gene therapy in only one eye, a comparison of the treated eyes and their untreated counterparts was performed using the paired nonparametric significance test of Wilcoxon.

SUPPLEMENTAL INFORMATION

Supplemental Information includes six figures and four tables and can be found with this article online at http://dx.doi.org/10.1016/j.omtm.2017.04.008.

AUTHOR CONTRIBUTIONS

Conceived and designed the experiments: H.C.-T., C.L., T.D., and M.C.-D. Performed the experiments: H.C.-T., C.L., S.A., D.R., E.R., J.D.-C., M.S., H.L., A. Mohammad, and M.C.-D. Analyzed the data: H.C.-T., S.A., C.L., J.D.-C., M.S., D.R., E.R., H.L., F.B.-B., A. Mohammad, A. Maron, T.D., H.L., and M.C.-D. Wrote the paper: H.C.-T., S.A., C.L., and M.C.-D.

CONFLICTS OF INTEREST

T.D. and A. Maron are employed by Sanofi Fovea-Ophthalmology, which supported the study. An international application for a patent has been filed on neuroglobin (PCT/FR2013/05232). The authors have no other patents, marketed products, or products in development to declare.

ACKNOWLEDGMENTS

We are grateful to David Godefroy and Stéphane Fouquet (Imaging Facility of the Vision Institute), Zsolt Csaba (Platform of Microscopy and Imaging of the UMR INSERM 1141), Jose-Alain Sahel (Director of the Vision Institute), and Pierre Gresens (Director of PROTECT, INSERM, Université Paris Diderot, Sorbonne Paris Cité, Paris, France). We thank Keith A. Laycock (St. Jude Children's Research Hospital) for editing the manuscript. We also thank Fovea Pharmaceuticals (Sanofi, Ophthalmology Division), the University Pierre and Marie Curie (UPMC), the National Institute of Health and Medical Research (INSERM), the National Center for Scientific Research (CNRS), LABEX LIFESENSES (Vision Institute), and the INSB (Institut National de Sciences Biologiques)-UNADEV (Union Nationale des Aveugles et Déficients Visuels).

REFERENCES

1. Tham, Y.C., Li, X., Wong, T.Y., Quigley, H.A., Aung, T., and Cheng, C.Y. (2014). Global prevalence of glaucoma and projections of glaucoma burden through 2040: a systematic review and meta-analysis. Ophthalmology *121*, 2081–2090.
2. Quigley, H.A., McKinnon, S.J., Zack, D.J., Pease, M.E., Kerrigan-Baumrind, L.A., Kerrigan, D.F., and Mitchell, R.S. (2000). Retrograde axonal transport of BDNF in retinal ganglion cells is blocked by acute IOP elevation in rats. Invest. Ophthalmol. Vis. Sci. *41*, 3460–3466.
3. Hwang, J.C., Konduru, R., Zhang, X., Tan, O., Francis, B.A., Varma, R., Sehi, M., Greenfield, D.S., Sadda, S.R., and Huang, D. (2012). Relationship among visual field, blood flow, and neural structure measurements in glaucoma. Invest. Ophthalmol. Vis. Sci. *53*, 3020–3026.
4. Hare, W., WoldeMussie, E., Lai, R., Ton, H., Ruiz, G., Feldmann, B., Wijono, M., Chun, T., and Wheeler, L. (2001). Efficacy and safety of memantine, an NMDA-type open-channel blocker, for reduction of retinal injury associated with experimental glaucoma in rat and monkey. Surv. Ophthalmol. *45*, S284–S289, discussion S295–S286.
5. Prasanna, G., Krishnamoorthy, R., and Yorio, T. (2011). Endothelin, astrocytes and glaucoma. Exp. Eye Res. *93*, 170–177.
6. Nita, M., and Grzybowski, A. (2016). The role of the reactive oxygen species and oxidative stress in the pathomechanism of the age-related ocular diseases and other pathologies of the anterior and posterior eye segments in adults. Oxid. Med. Cell. Longev. *2016*, 3164734.
7. Liu, Y., and Pang, I.H. (2013). Challenges in the development of glaucoma neuroprotection therapy. Cell Tissue Res. *353*, 253–260.
8. Quigley, H.A. (2011). Glaucoma. Lancet *377*, 1367–1377.
9. Yu, D.Y., Cringle, S.J., Balaratnasingam, C., Morgan, W.H., Yu, P.K., and Su, E.N. (2013). Retinal ganglion cells: Energetics, compartmentation, axonal transport, cytoskeletons and vulnerability. Prog. Retin. Eye Res. *36*, 217–246.
10. Lee, S., Sheck, L., Crowston, J.G., Van Bergen, N.J., O'Neill, E.C., O'Hare, F., Kong, Y.X., Chrysostomou, V., Vincent, A.L., and Trounce, I.A. (2012). Impaired complex-I-linked respiration and ATP synthesis in primary open-angle glaucoma patient lymphoblasts. Invest. Ophthalmol. Vis. Sci. *53*, 2431–2437.
11. Van Bergen, N.J., Crowston, J.G., Craig, J.E., Burdon, K.P., Kearns, L.S., Sharma, S., Hewitt, A.W., Mackey, D.A., and Trounce, I.A. (2015). Measurement of systemic mitochondrial function in advanced primary open-angle glaucoma and Leber hereditary optic neuropathy. PLoS ONE *10*, e0140919.
12. Lascaratos, G., Chau, K.Y., Zhu, H., Gkotsi, D., King, R., Gout, I., Kamal, D., Luthert, P.J., Schapira, A.H., and Garway-Heath, D.F. (2015). Resistance to the most common optic neuropathy is associated with systemic mitochondrial efficiency. Neurobiol. Dis. *82*, 78–85.
13. Osborne, N.N., Núñez-Álvarez, C., Joglar, B., and Del Olmo-Aguado, S. (2016). Glaucoma: Focus on mitochondria in relation to pathogenesis and neuroprotection. Eur. J. Pharmacol. *787*, 127–133.

14. Burmester, T., Weich, B., Reinhardt, S., and Hankeln, T. (2000). A vertebrate globin expressed in the brain. Nature *407*, 520–523.

15. Li, R.C., Guo, S.Z., Lee, S.K., and Gozal, D. (2010). Neuroglobin protects neurons against oxidative stress in global ischemia. J. Cereb. Blood Flow Metab. *30*, 1874–1882.

16. Lechauve, C., Rezaei, H., Celier, C., Kiger, L., Corral-Debrinski, M., Noinville, S., Chauvierre, C., Hamdane, D., Pato, C., and Marden, M.C. (2009). Neuroglobin and prion cellular localization: investigation of a potential interaction. J. Mol. Biol. *388*, 968–977.

17. Lechauve, C., Augustin, S., Roussel, D., Sahel, J.A., and Corral-Debrinski, M. (2013). Neuroglobin involvement in visual pathways through the optic nerve. Biochim. Biophys. Acta *1834*, 1772–1778.

18. Lechauve, C., Augustin, S., Cwerman-Thibault, H., Bouaita, A., Forster, V., Célier, C., Rustin, P., Marden, M.C., Sahel, J.A., and Corral-Debrinski, M. (2012). Neuroglobin involvement in respiratory chain function and retinal ganglion cell integrity. Biochim. Biophys. Acta *1823*, 2261–2273.

19. Klein, J.A., Longo-Guess, C.M., Rossmann, M.P., Seburn, K.L., Hurd, R.E., Frankel, W.N., Bronson, R.T., and Ackerman, S.L. (2002). The harlequin mouse mutation downregulates apoptosis-inducing factor. Nature *419*, 367–374.

20. Lechauve, C., Augustin, S., Cwerman-Thibault, H., Reboussin, É., Roussel, D., Lai-Kuen, R., Saubamea, B., Sahel, J.A., Debeir, T., and Corral-Debrinski, M. (2014). Neuroglobin gene therapy prevents optic atrophy and preserves durably visual function in *Harlequin* mice. Mol. Ther. *22*, 1096–1109.

21. Anderson, M.G., Smith, R.S., Hawes, N.L., Zabaleta, A., Chang, B., Wiggs, J.L., and John, S.W. (2002). Mutations in genes encoding melanosomal proteins cause pigmentary glaucoma in DBA/2J mice. Nat. Genet. *30*, 81–85.

22. Libby, R.T., Anderson, M.G., Pang, I.H., Robinson, Z.H., Savinova, O.V., Cosma, I.M., Snow, A., Wilson, L.A., Smith, R.S., Clark, A.F., and John, S.W. (2005). Inherited glaucoma in DBA/2J mice: pertinent disease features for studying the neurodegeneration. Vis. Neurosci. *22*, 637–648.

23. Jakobs, T.C., Libby, R.T., Ben, Y., John, S.W., and Masland, R.H. (2005). Retinal ganglion cell degeneration is topological but not cell type specific in DBA/2J mice. J. Cell Biol. *171*, 313–325.

24. Moon, J.I., Kim, I.B., Gwon, J.S., Park, M.H., Kang, T.H., Lim, E.J., Choi, K.R., and Chun, M.H. (2005). Changes in retinal neuronal populations in the DBA/2J mouse. Cell Tissue Res. *320*, 51–59.

25. Wong, A.A., and Brown, R.E. (2007). Age-related changes in visual acuity, learning and memory in C57BL/6J and DBA/2J mice. Neurobiol. Aging *28*, 1577–1593.

26. Zhou, X., Li, F., Kong, L., Tomita, H., Li, C., and Cao, W. (2005). Involvement of inflammation, degradation, and apoptosis in a mouse model of glaucoma. J. Biol. Chem. *280*, 31240–31248.

27. Nadal-Nicolás, F.M., Jiménez-López, M., Salinas-Navarro, M., Sobrado-Calvo, P., Alburquerque-Béjar, J.J., Vidal-Sanz, M., and Agudo-Barriuso, M. (2012). Whole number, distribution and co-expression of brn3 transcription factors in retinal ganglion cells of adult albino and pigmented rats. PLoS ONE *7*, e49830.

28. Schlamp, C.L., Li, Y., Dietz, J.A., Janssen, K.T., and Nickells, R.W. (2006). Progressive ganglion cell loss and optic nerve degeneration in DBA/2J mice is variable and asymmetric. BMC Neurosci. *7*, 66.

29. Buckingham, B.P., Inman, D.M., Lambert, W., Oglesby, E., Calkins, D.J., Steele, M.R., Vetter, M.L., Marsh-Armstrong, N., and Horner, P.J. (2008). Progressive ganglion cell degeneration precedes neuronal loss in a mouse model of glaucoma. J. Neurosci. *28*, 2735–2744.

30. Wang, J., and Dong, Y. (2016). Characterization of intraocular pressure pattern and changes of retinal ganglion cells in DBA2J glaucoma mice. Int. J. Ophthalmol. *9*, 211–217.

31. Chen, H., and Weber, A.J. (2002). Expression of glial fibrillary acidic protein and glutamine synthetase by Müller cells after optic nerve damage and intravitreal application of brain-derived neurotrophic factor. Glia *38*, 115–125.

32. Fernández-Sánchez, L., de Sevilla Müller, L.P., Brecha, N.C., and Cuenca, N. (2014). Loss of outer retinal neurons and circuitry alterations in the DBA/2J mouse. Invest. Ophthalmol. Vis. Sci. *55*, 6059–6072.

33. Bénit, P., Goncalves, S., Philippe Dassa, E., Brière, J.J., Martin, G., and Rustin, P. (2006). Three spectrophotometric assays for the measurement of the five respiratory chain complexes in minuscule biological samples. Clin. Chim. Acta *374*, 81–86.

34. Salinas-Navarro, M., Mayor-Torroglosa, S., Jiménez-López, M., Avilés-Trigueros, M., Holmes, T.M., Lund, R.D., Villegas-Pérez, M.P., and Vidal-Sanz, M. (2009). A computerized analysis of the entire retinal ganglion cell population and its spatial distribution in adult rats. Vision Res. *49*, 115–126.

35. Johnson, J.E., Jr., Perkins, G.A., Giddabasappa, A., Chaney, S., Xiao, W., White, A.D., Brown, J.M., Waggoner, J., Ellisman, M.H., and Fox, D.A. (2007). Spatiotemporal regulation of ATP and Ca^{2+} dynamics in vertebrate rod and cone ribbon synapses. Mol. Vis. *13*, 887–919.

36. Kim, K.Y., Perkins, G.A., Shim, M.S., Bushong, E., Alcasid, N., Ju, S., Ellisman, M.H., Weinreb, R.N., and Ju, W.K. (2015). DRP1 inhibition rescues retinal ganglion cells and their axons by preserving mitochondrial integrity in a mouse model of glaucoma. Cell Death Dis. *6*, e1839.

37. Siu, T.L., and Morley, J.W. (2008). Suppression of visual cortical evoked responses following deprivation of pattern vision in adult mice. Eur. J. Neurosci. *28*, 484–490.

38. Heiduschka, P., Julien, S., Schuettauf, F., and Schnichels, S. (2010). Loss of retinal function in aged DBA/2J mice - New insights into retinal neurodegeneration. Exp. Eye Res. *91*, 779–783.

39. Sullivan, T.A., Geisert, E.E., Hines-Beard, J., and Rex, T.S. (2011). Systemic adeno-associated virus-mediated gene therapy preserves retinal ganglion cells and visual function in DBA/2J glaucomatous mice. Hum. Gene Ther. *22*, 1191–1200.

40. Tanimoto, N., Sothilingam, V., and Seeliger, M.W. (2013). Functional phenotyping of mouse models with ERG. Methods Mol. Biol. *935*, 69–78.

41. Neveu, M.M., and Jeffery, G. (2007). Chiasm formation in man is fundamentally different from that in the mouse. Eye (Lond.) *21*, 1264–1270.

42. M, K. (2015). Present and new treatment strategies in the management of glaucoma. Open Ophthalmol. J. *9*, 89–100.

43. Barron, M.J., Griffiths, P., Turnbull, D.M., Bates, D., and Nichols, P. (2004). The distributions of mitochondria and sodium channels reflect the specific energy requirements and conduction properties of the human optic nerve head. Br. J. Ophthalmol. *88*, 286–290.

44. Schuettauf, F., Rejdak, R., Walski, M., Frontczak-Baniewicz, M., Voelker, M., Blatsios, G., Shinoda, K., Zagorski, Z., Zrenner, E., and Grieb, P. (2004). Retinal neurodegeneration in the DBA/2J mouse-a model for ocular hypertension. Acta Neuropathol. *107*, 352–358.

45. Baltan, S., Inman, D.M., Danilov, C.A., Morrison, R.S., Calkins, D.J., and Horner, P.J. (2010). Metabolic vulnerability disposes retinal ganglion cell axons to dysfunction in a model of glaucomatous degeneration. J. Neurosci. *30*, 5644–5652.

46. Son, J.L., Soto, I., Oglesby, E., Lopez-Roca, T., Pease, M.E., Quigley, H.A., and Marsh-Armstrong, N. (2010). Glaucomatous optic nerve injury involves early astrocyte reactivity and late oligodendrocyte loss. Glia *58*, 780–789.

47. Funke, S., Perumal, N., Beck, S., Gabel-Scheurich, S., Schmelter, C., Teister, J., Gerbig, C., Gramlich, O.W., Pfeiffer, N., and Grus, F.H. (2016). Glaucoma related proteomic alterations in human retina samples. Sci. Rep. *6*, 29759.

48. Yang, X., Hondur, G., Li, M., Cai, J., Klein, J.B., Kuehn, M.H., and Tezel, G. (2015). Proteomics analysis of molecular risk factors in the ocular hypertensive human retina. Invest. Ophthalmol. Vis. Sci. *56*, 5816–5830.

49. Fiocchetti, M., De Marinis, E., Ascenzi, P., and Marino, M. (2013). Neuroglobin and neuronal cell survival. Biochim. Biophys. Acta *1834*, 1744–1749.

50. Hundahl, C.A., Fahrenkrug, J., Luuk, H., Hay-Schmidt, A., and Hannibal, J. (2012). Restricted expression of neuroglobin in the mouse retina and co-localization with melanopsin and tyrosine hydroxylase. Biochem. Biophys. Res. Commun. *425*, 100–106.

51. Rajendram, R., and Rao, N.A. (2007). Neuroglobin in normal retina and retina from eyes with advanced glaucoma. Br. J. Ophthalmol. *91*, 663–666.

52. Ostojić, J., Grozdanić, S.D., Syed, N.A., Hargrove, M.S., Trent, J.T., 3rd, Kuehn, M.H., Kwon, Y.H., Kardon, R.H., and Sakaguchi, D.S. (2008). Patterns of distribution of oxygen-binding globins, neuroglobin and cytoglobin in human retina. Arch. Ophthalmol. *126*, 1530–1536.

53. Guidolin, D., Tortorella, C., Marcoli, M., Maura, G., and Agnati, L.F. (2016). Neuroglobin, a factor playing for nerve cell survival. Int. J. Mol. Sci. *17*, 1817.

54. Trashin, S., de Jong, M., Luyckx, E., Dewilde, S., and De Wael, K. (2016). Electrochemical evidence for neuroglobin activity on NO at physiological concentrations. J. Biol. Chem. *291*, 18959–18966.

55. Guidolin, D., Agnati, L.F., Tortorella, C., Marcoli, M., Maura, G., Albertin, G., and Fuxe, K. (2014). Neuroglobin as a regulator of mitochondrial-dependent apoptosis: a bioinformatics analysis. Int. J. Mol. Med. *33*, 111–116.

56. Bønding, S.H., Henty, K., Dingley, A.J., and Brittain, T. (2008). The binding of cytochrome c to neuroglobin: a docking and surface plasmon resonance study. Int. J. Biol. Macromol. *43*, 295–299.

57. Brittain, T., Skommer, J., Raychaudhuri, S., and Birch, N. (2010). An antiapoptotic neuroprotective role for neuroglobin. Int. J. Mol. Sci. *11*, 2306–2321.

58. Yu, Z., Zhang, Y., Liu, N., Yuan, J., Lin, L., Zhuge, Q., Xiao, J., and Wang, X. (2016). Roles of neuroglobin binding to mitochondrial complex III subunit cytochrome c1 in oxygen-glucose deprivation–induced neurotoxicity in primary neurons. Mol. Neurobiol. *53*, 3249–3257.

59. Vahsen, N., Candé, C., Brière, J.J., Bénit, P., Joza, N., Larochette, N., Mastroberardino, P.G., Pequignot, M.O., Casares, N., Lazar, V., et al. (2004). AIF deficiency compromises oxidative phosphorylation. EMBO J. *23*, 4679–4689.

60. Sauvé, Y., Sawai, H., and Rasminsky, M. (1995). Functional synaptic connections made by regenerated retinal ganglion cell axons in the superior colliculus of adult hamsters. J. Neurosci. *15*, 665–675.

61. Georgiou, A.L., Guo, L., Cordeiro, M.F., and Salt, T.E. (2010). Changes in NMDA receptor contribution to synaptic transmission in the brain in a rat model of glaucoma. Neurobiol. Dis. *39*, 344–351.

62. Georgiou, A.L., Guo, L., Cordeiro, M.F., and Salt, T.E. (2012). Changes in the modulation of retinocollicular transmission through group III mGluRs long after an increase in intraocular pressure in a rat model of glaucoma. Vis. Neurosci. *29*, 237–246.

63. Park, H.Y., Kim, J.H., and Park, C.K. (2014). Alterations of the synapse of the inner retinal layers after chronic intraocular pressure elevation in glaucoma animal model. Mol. Brain *7*, 53.

64. Sun, T., Qiao, H., Pan, P.Y., Chen, Y., and Sheng, Z.H. (2013). Motile axonal mitochondria contribute to the variability of presynaptic strength. Cell Rep. *4*, 413–419.

65. Schultz, B.R., and Chamberlain, J.S. (2008). Recombinant adeno-associated virus transduction and integration. Mol. Ther. *16*, 1189–1199.

66. Pauly, A., Brignole-Baudouin, F., Labbé, A., Liang, H., Warnet, J.M., and Baudouin, C. (2007). New tools for the evaluation of toxic ocular surface changes in the rat. Invest. Ophthalmol. Vis. Sci. *48*, 5473–5483.

67. Jammoul, F., Wang, Q., Nabbout, R., Coriat, C., Duboc, A., Simonutti, M., Dubus, E., Craft, C.M., Ye, W., Collins, S.D., et al. (2009). Taurine deficiency is a cause of vigabatrin-induced retinal phototoxicity. Ann. Neurol. *65*, 98–107.

68. Ridder, W.H., 3rd, and Nusinowitz, S. (2006). The visual evoked potential in the mouse–origins and response characteristics. Vision Res. *46*, 902–913.

69. Chou, T.H., Kocaoglu, O.P., Borja, D., Ruggeri, M., Uhlhorn, S.R., Manns, F., and Porciatti, V. (2011). Postnatal elongation of eye size in DBA/2J mice compared with C57BL/6J mice: in vivo analysis with whole-eye OCT. Invest. Ophthalmol. Vis. Sci. *52*, 3604–3612.

70. Jayaraman, T., Tejero, J., Chen, B.B., Blood, A.B., Frizzell, S., Shapiro, C., Tiso, M., Hood, B.L., Wang, X., Zhao, X., et al. (2011). 14-3-3 binding and phosphorylation of neuroglobin during hypoxia modulate six-to-five heme pocket coordination and rate of nitrite reduction to nitric oxide. J. Biol. Chem. *286*, 42679–42689.

71. Schmidt, M., Giessl, A., Laufs, T., Hankeln, T., Wolfrum, U., and Burmester, T. (2003). How does the eye breathe? Evidence for neuroglobin-mediated oxygen supply in the mammalian retina. J. Biol. Chem. *278*, 1932–1935.

OMTM, Volume *5*

Supplemental Information

Neuroglobin Can Prevent or Reverse Glaucomatous Progression in DBA/2J Mice

Hélène Cwerman-Thibault, Christophe Lechauve, Sébastien Augustin, Delphine Roussel, Élodie Reboussin, Ammara Mohammad, Julie Degardin-Chicaud, Manuel Simonutti, Hong Liang, Françoise Brignole-Baudouin, Anne Maron, Thomas Debeir, and Marisol Corral-Debrinski

Figure S1

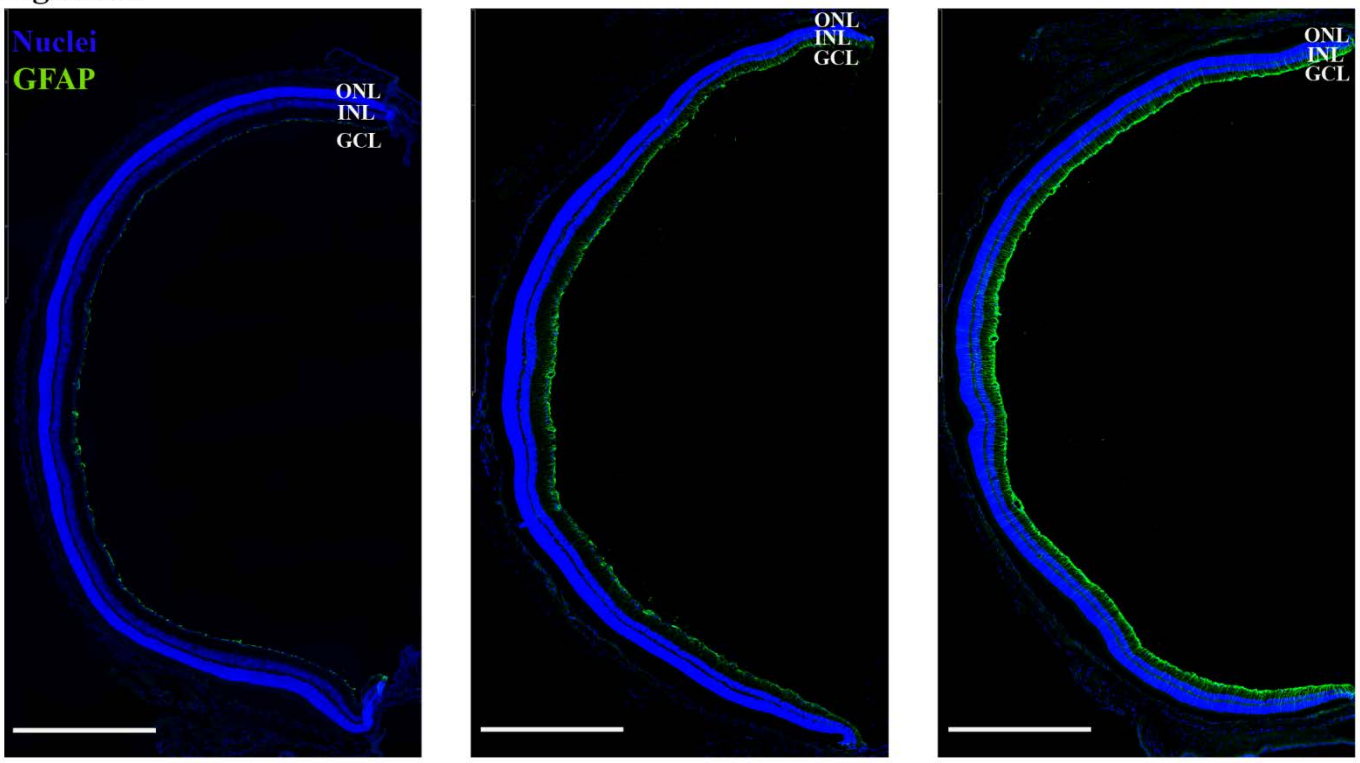

Untreated retina, 2-month-old DBA/2J | Untreated retina, 8-month-old DBA/2J | Untreated retina, 12-month-old DBA/2J

Figure S2

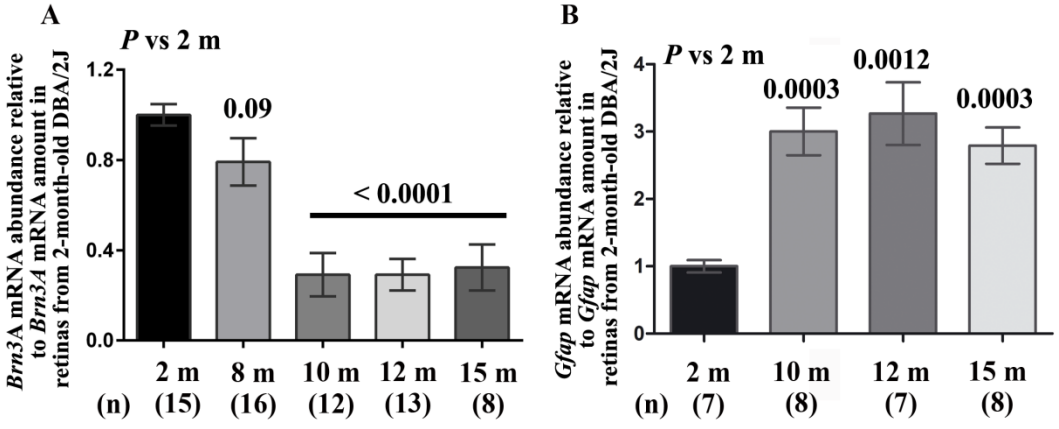

Figure S3

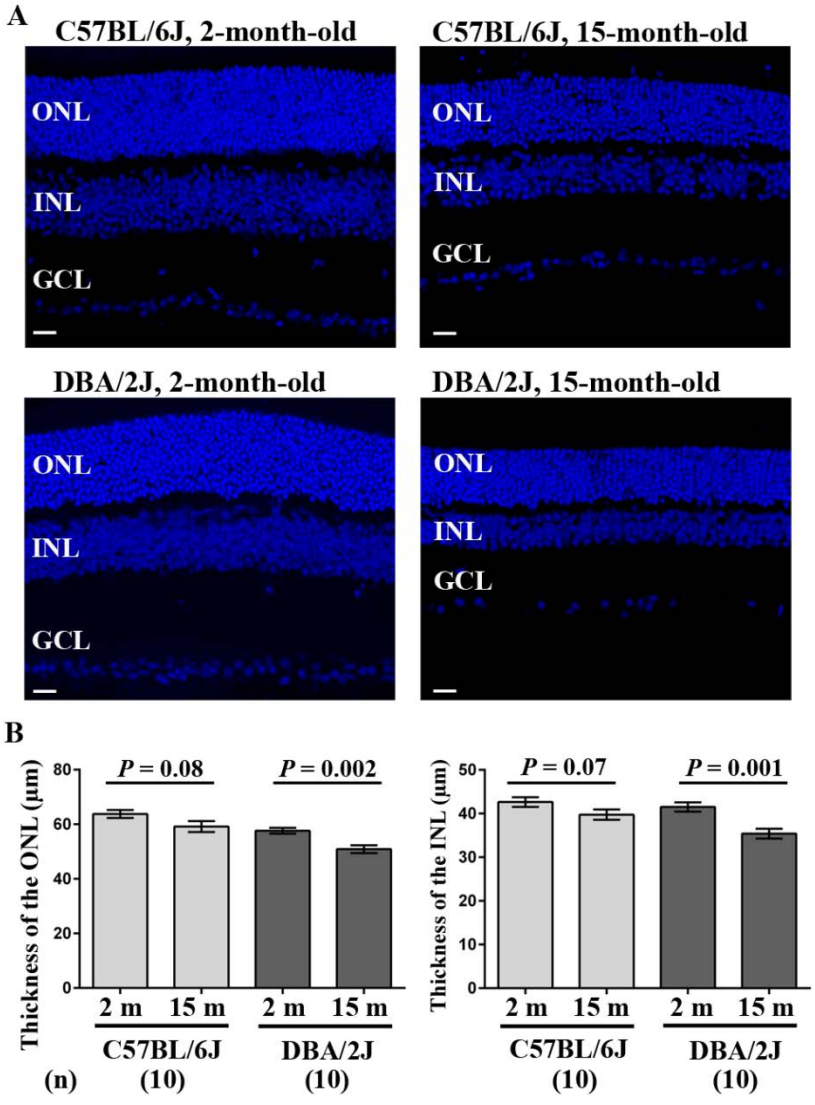
A
C57BL/6J, 2-month-old
C57BL/6J, 15-month-old
DBA/2J, 2-month-old
DBA/2J, 15-month-old
ONL
INL
GCL
B
Thickness of the ONL (μm)
P = 0.08
P = 0.002
Thickness of the INL (μm)
P = 0.07
P = 0.001
2 m
15 m
C57BL/6J
DBA/2J
(n)
(10)

Figure S4

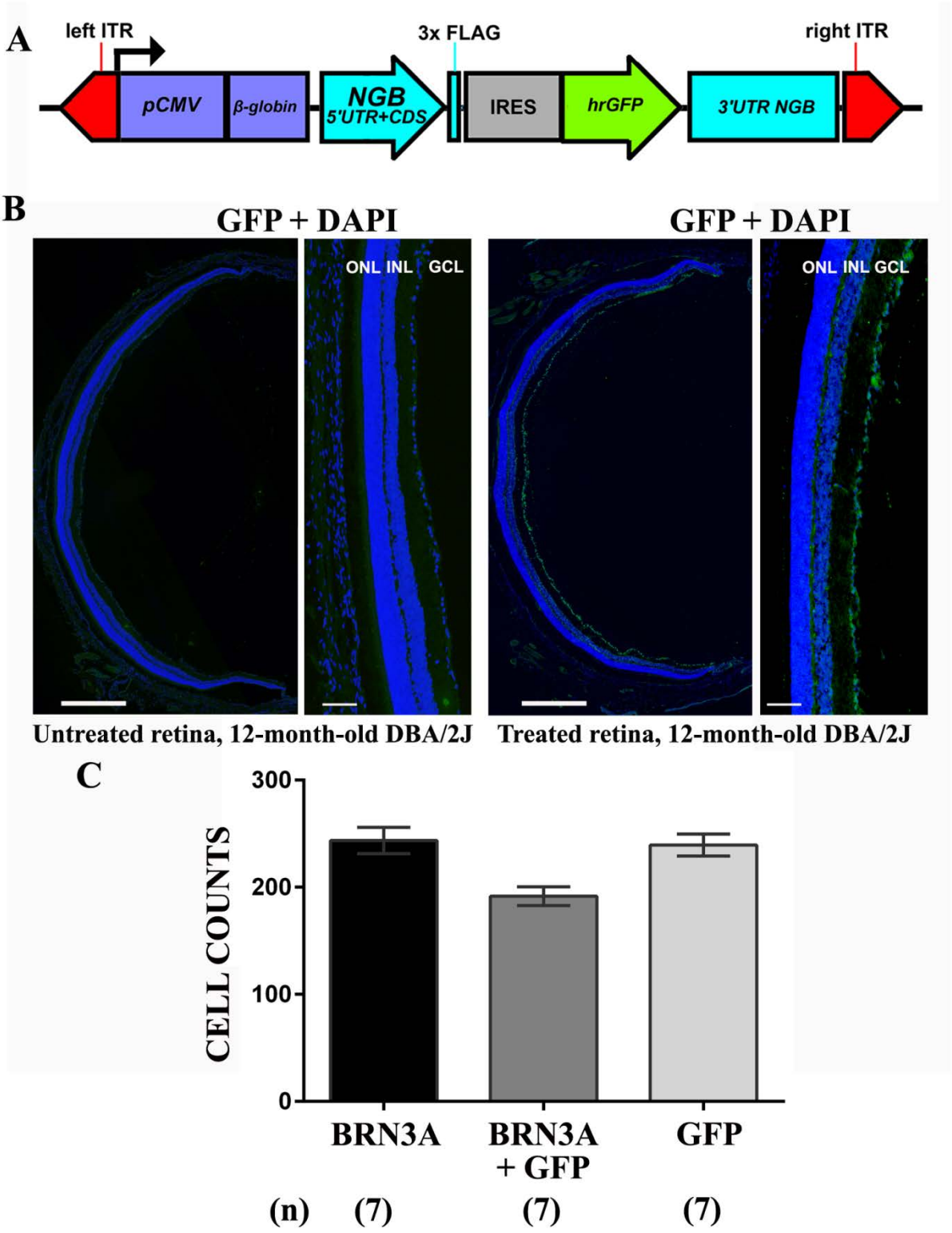
A
left ITR
3x FLAG
right ITR
pCMV
β-globin
NGB
5'UTR+CDS
IRES
hrGFP
3'UTR NGB
B
GFP + DAPI
GFP + DAPI
ONL INL GCL
ONL INL GCL
Untreated retina, 12-month-old DBA/2J
Treated retina, 12-month-old DBA/2J
C
CELL COUNTS
300
200
100
0
BRN3A
BRN3A + GFP
GFP
(n) (7) (7) (7)

Figure S5

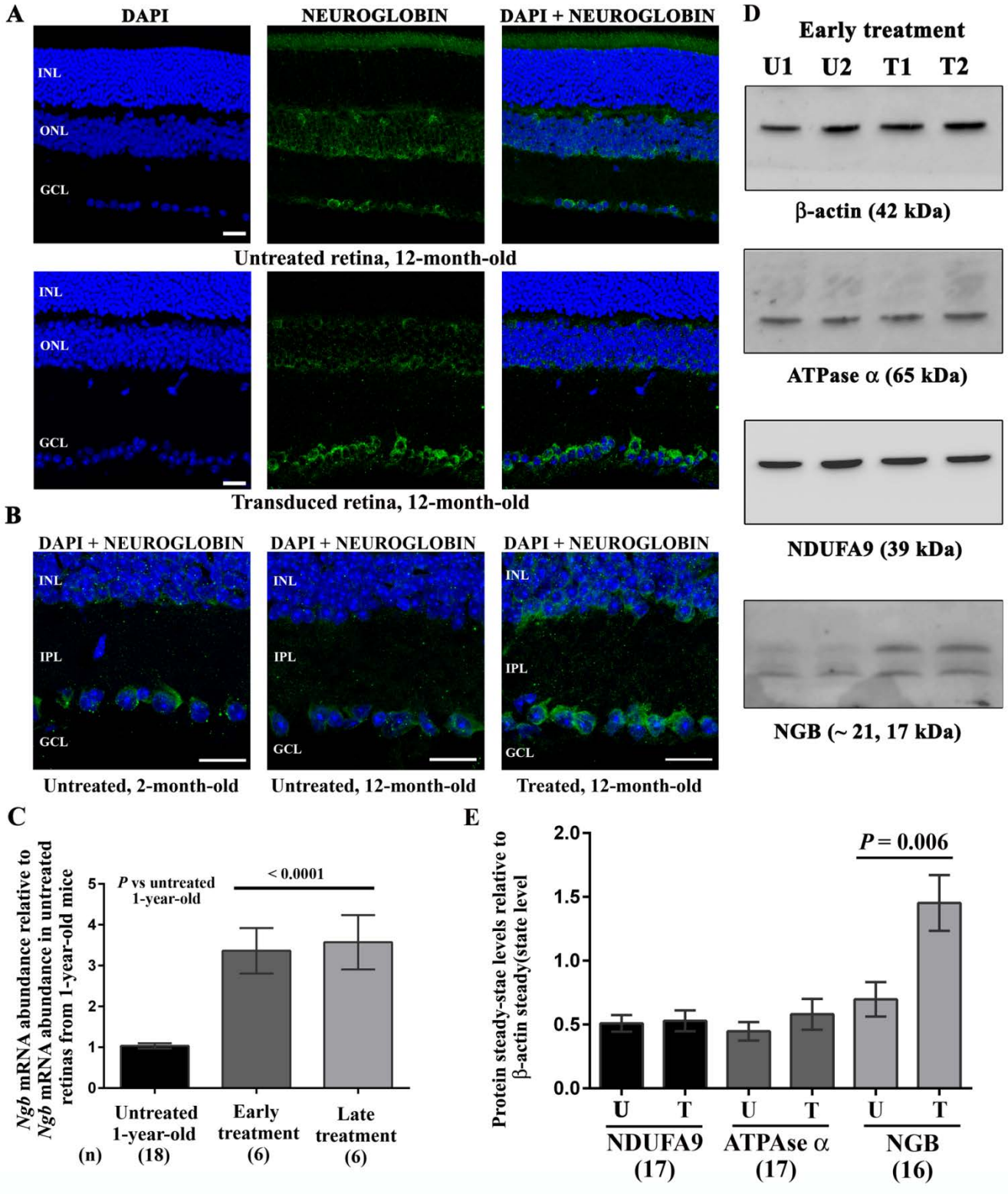
A
DAPI
NEUROGLOBIN
DAPI + NEUROGLOBIN
INL
ONL
GCL
Untreated retina, 12-month-old
Transduced retina, 12-month-old
B
DAPI + NEUROGLOBIN
IPL
Untreated, 2-month-old
Untreated, 12-month-old
Treated, 12-month-old
C
Ngb mRNA abundance relative to Ngb mRNA abundance in untreated retinas from 1-year-old mice
P vs untreated 1-year-old
< 0.0001
Untreated 1-year-old
Early treatment
Late treatment
(n)
(18)
(6)
(6)
D
Early treatment
U1
U2
T1
T2
β-actin (42 kDa)
ATPase α (65 kDa)
NDUFA9 (39 kDa)
NGB (~ 21, 17 kDa)
E
Protein steady-stae levels relative to β-actin steady(state level
P = 0.006
U
T
NDUFA9 (17)
ATPase α (17)
NGB (16)

Figure S6

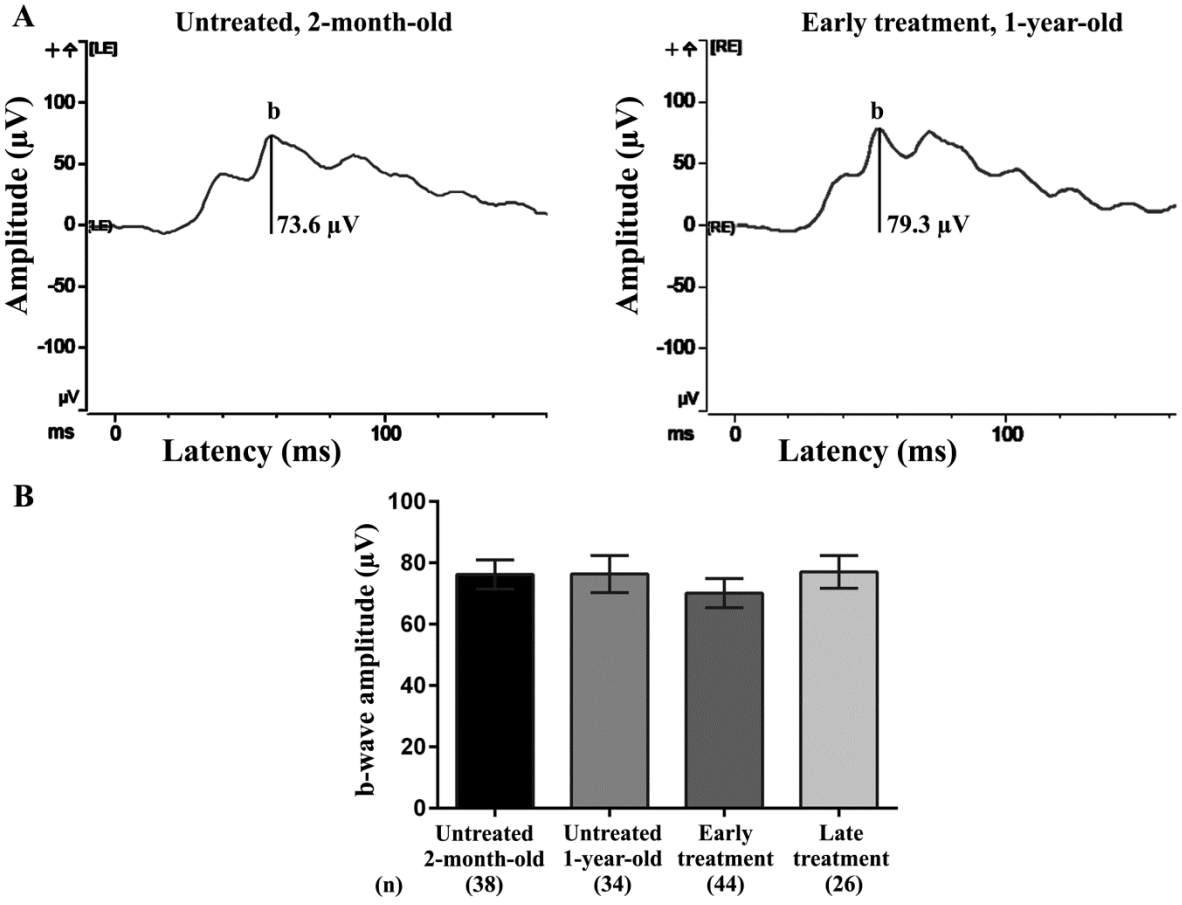
A
Untreated, 2-month-old
Early treatment, 1-year-old
[LE]
[RE]
b
73.6 µV
79.3 µV
Amplitude (µV)
100
50
0
-50
-100
µV
ms
0
100
Latency (ms)
B
b-wave amplitude (µV)
100
80
60
40
20
0
Untreated 2-month-old
Untreated 1-year-old
Early treatment
Late treatment
(n)
(38)
(34)
(44)
(26)

FIGURE LEGENDS

Figure S1: Glial fibrillary acidic protein abundance in retinas of DBA/2J mice at different ages.

The results of immunohistochemical staining for GFAP (green) and the reconstruction of whole retinal sections from untreated mice aged 2, 8, and 12 months are shown. The reconstruction of retinal sections was performed with the NDP 2.0 HT scanner. Cell nuclei were stained with DAPI (blue). The scale bars correspond to 5 mm.

Figure S2: *Brn3A* and *Gfap* expression in retinas of DBA/2J mice at different ages.

RT-qPCR assays were performed using total RNA extracted from retinas isolated from DBA/2J mice aged between 2 and 15 months. The histograms show the steady-state levels of *Brn3a* and *Gfap* mRNAs as the means ± SEMs after normalization of the signals against the mean signals for *Brn3a* and *Gfap* mRNAs in retinas from 2-month-old mice. The number of independent RNAs assessed per group is indicated in brackets below each bar. The primers used are shown in Table S4. The *P*-values shown were calculated with respect to data collected from untreated 2-month-old DBA/2J mice and plotted using GraphPad Prism 6.

Figure S3: Assessment of the thickness of neuronal cell layers in retinas of C57BL/6J and DBA/2J mice.

(A) Confocal images of retinal sections stained with DAPI from C57BL/6J and DBA/2J mice aged 2 months (2 m) or 15 months (15 m). The scale bars correspond to 20 μm. Abbreviations: GCL, ganglion cell layer; INL, inner nuclear layer; ONL, outer nuclear layer.

(B) The thickness of the ONLs and INLs was estimated using the NDP 2.0 HT scanner and the associated software after reconstructing the entire retinal sections from five C57BL/6J mice aged 2 months, five C57BL/6J mice aged 15 months, five DBA/2J mice aged 2 months, and five DBA/2J mice aged 15 months. The measurements were performed at two central points for each section, and two or three sections were evaluated for each animal. A total of 10 independent retinas were analyzed for each group. Bar graphs of the

thickness in μm for the ONLs and INLs were produced with GraphPad Prism 6, with the values plotted as means ± SEMs. *P*-values were calculated by comparing the values obtained for mice aged 2 and 15 months for the two strains evaluated.

Figure S4: AAV2/2-*NGB* vector map and transduction yield after a single intravitreal injection.

A) Physical map of the AAV2/2-*NGB* vector genome (7255 bp), encompassing mouse *NGB* sequences inserted into the *pAAV-IRES-hrGFP* plasmid: the NGB ORF (453 bp), encoding 151 amino acids (CDS), is in frame with three FLAG epitopes and is transcribed under the control of the cytomegalovirus promoter (pCMV) and the β-globin intron. The construct contains the untranslated regions at the 5′ (279 bp) and 3′ (895 bp) ends of the mouse *Ngb* mRNA (NM_022414.2). The plasmid also contains a cassette that allows the expression of the recombinant humanized green fluorescent protein (GFP) translated from the encephalomyocarditis virus internal ribosome entry site.

(B) Transduction efficiency was evaluated by immunohistochemical staining for GFP in sections of retinas from DBA/2J mice euthanized 10 months after undergoing a single intravitreal injection of AAV2/2-*NGB* (2 × 109 VG in one eye). Labeling for GFP is shown in green; cell nuclei were stained with DAPI (blue). The scale bars correspond to 2.5 mm and (in the magnification) 50 μm. Abbreviations: GCL, ganglion cell layer; INL, inner nuclear layer; ONL, outer nuclear layer.

(C) The histogram shows the numerical evaluation of the data illustrated in (B). Mice underwent intravitreal injection of AAV2/2-*NGB* at the age of 2 months (early treatment) and were euthanized 10 months later. Three or four independent sections from each of seven treated eyes were examined to estimate the number of (a) RGCs (BRN3A-positive cells), (b) transduced cells in the GCL (GFP-positive cells), and (c) transduced RGCs (BRN3A and GFP positive cells). The histogram, prepared using GraphPad Prism 6, shows the means ± SEMs obtained for the seven mice.

Figure S5: *Ngb* expression in retinas of mice treated with AAV2/2-*NGB*.

(A) The results of immunofluorescence analysis using the anti-NGB antibody (green), showing retinal sections from a single 1-year-old DBA/2J mouse that underwent AAV2/2-*NGB* intravitreal injection in one eye at 2 months of age while the contralateral eye remained untreated. The nuclei were stained with DAPI (blue). The scale bars correspond to 20 μm. Abbreviations: ONL, outer nuclear layer; INL, inner nuclear layer; GCL, ganglion cell layer.

(B) Confocal images of retinal sections subjected to immunohistochemical staining for NGB are shown as composites of NGB (green) and DAPI (blue) signals. They correspond to retinal sections from two untreated mice aged 2 and 12 months, respectively, and a treated animal that received early treatment and was euthanized at 12 months of age. The scale bars correspond to 20 μm. Abbreviations: ONL, outer nuclear layer; INL, inner nuclear layer; GCL, ganglion cell layer.

(C) RT-qPCR assays were performed with total RNA extracted from 17 retinas from 1-year-old untreated mice, six retinas from the treated eyes of mice that received early treatment, and six retinas from mice that received late treatment. The primers used are shown in Table S4. The bar chart shows the steady-state levels of *Ngb* mRNA relative to the values assessed in retinal RNAs purified from 1-year-old untreated mice. The *P*-values were calculated with GraphPad Prism 6.

(D) Representative Western blots obtained from two pairs of retinas isolated from 1-year-old mice that received early treatment in only one eye (T) and from their contralateral untreated counterparts (U). The membranes were successively incubated with antibodies against NGB, NDUFA9, ATP synthase α, and β-actin (as the loading control). Seven pairs of retinas from mice that were euthanized at 1 year of age and in which only one eye underwent vector administration at the age of 2 months were assessed. As seen in Figure 5, staining with antibody against NGB revealed two main signals, with apparent molecular masses of 21 and 17 kDa, and also a faint band between the two main bands.

(E) Bar chart showing the relative amounts of NGB, NDUFA9, and ATP synthase α in retinas from untreated and treated eyes. The intensities of the NGB signals were normalized against β-actin signals; the number of individual signals is indicated in brackets (n). No treatment-linked difference was noticed in the abundance

of NDUFA9 or ATP synthase α, whereas there was a twofold increase in NGB abundance in retinas from the treated eyes of mice. This difference was significant when the results were compared to those obtained in age-matched untreated retinas ($P = 0.006$).

Figure S6: Light-adapted electroretinograms recorded in mice treated with AAV2/2-*NGB*.

(A) Plots of light-adapted ERG responses recorded in two DBA/2J mice: one 2-month-old untreated mouse and 12-month-old mouse that had undergone an injection of AAV2/2-*NGB* in one eye at the age of 2 months. (B) ERG responses are represented in the bar chart as means ± SEMs for each group evaluated. There were no statistically significant differences between the data for the different groups. The number of individual responses recorded for each group is indicated in brackets below each bar (n).

Table S1: Electroretinogram and flash visual evoked potential components in DBA/2J mice

	Untreated 2-month-old mice ± SEM (n = 38)	Untreated 12-month-old mice ± SEM (n = 34)	Treated mice at 2 months ± SEM (n = 44)	Treated mice at 8 months ± SEM (n = 26)
Amplitude of b-wave (µV)	76.22 ± 4.8	76.37 ± 6.03	70.11 ± 4.73	77.02 ± 5.32
Latency of b-wave (ms)	69.72 ± 2.66	61.21 ± 1.86	61.76 ± 1.59	59.42 ± 1.45
Amplitude of N1 wave (µV)	46.95 ± 4.1	27.1 ± 4.51	50.9 ± 4.96	51.4 ± 4.86
Latency of N1 wave (ms)	68.04 ± 2.2	69.9 ± 2.7	72.7 ± 2.2	68.1 ± 1.7
Amplitude of P1 wave (µV)	58.6 ± 6.4	52.6 ± 8.9	46.9 ± 3.5	48.1 ± 6.13
Latency of P1 wave (ms)	111.2 ± 4.5	122.3 ± 4.7	116.2 ± 3.13	113.3 ± 2.84

The b-wave values shown correspond to photopic ERG recordings.

The N1 and P1 waves correspond to F-VEP responses.

The number of individual recordings is indicated in brackets.

Table S2: Antibody descriptions

Antibody target or reagent	Type	Assay: concentration	Supplier, catalog no.
BRN3A	Monoclonal	IIF: 8 µg/mL	Chemicon, MAB1585
GFP	Polyclonal	IIF:1.5 µg/mL	Torrey Pines Biolabs, TP401
NGB	Polyclonal	IIF: 5 µg/mL	Sigma-Aldrich, N-7162
NGB	Polyclonal	Western: 2 µg/mL	BioVendor, RD181043050
NGB	Polyclonal	Western: 1 µg/mL	Santa Cruz, Sc-30144
ATP synthase subunit α	Monoclonal	IIF: 2 µg/mL Western: 0.5 µg/mL	Thermo Fisher, 459240
β-actin	Monoclonal	Western: 0.2 µg/mL	Sigma-Aldrich, A5316
SOD2	Polyclonal	Western: 0.5 µg/mL	Abcam, ab13534
OPA1	Polyclonal	IIF: 5 µg/mL Western: 0.5 µg/mL	Abcam, ab42364
TOMM20	Monoclonal	IIF: 5 µg/mL Western: 1.25 µg/mL	Abcam, ab56783
NDUFA9	Monoclonal	IIF: 10 µg/mL Western: 1 µg/mL	Life Technologies, 459100
HSP60	Polyclonal	Western: 0.05 µg/mL	Abcam, ab46798

CytC	Monoclonal	IIF: 5 µg/mL Western: 2 µg/mL	Abcam, ab13575
AIF	Polyclonal	IIF: 2.5 µg/mL Western: 0.05 µg/mL	Abcam, ab32516
GFAP	Polyclonal	IIF: 3 µg/mL	Sigma-Aldrich, G3893
NF200	Polyclonal	IIF: 1 µg/mL	Sigma-Aldrich, N4142
IBA1	Polyclonal	IIF: 5 µg/mL	Wako, 019-19741
Vimentin	Monoclonal	IIF: 2.5 µg/mL	BD Pharmingen, 550513
Alexa 488	Anti-IgG, rabbit	IIF: 4 µg/mL	Life Technologies, A11008
Alexa 594	Anti-IgG, mouse	IIF: 4 µg/mL	Life Technologies, A11005
Goat anti-rabbit IgG	Goat anti-rabbit IgG, horseradish peroxidase conjugate	Western: 0.05 µg/mL	Jackson ImmunoResearch Laboratories, 111-035-144
Goat anti-mouse IgG	Goat anti-mouse IgG, horseradish peroxidase conjugate	Western: 0.05 µg/mL	Jackson ImmunoResearch Laboratories, 115-035-003
DAPI (4',6-diamidino-2-phenylindole, dihydrochloride)	Nucleic acid stain	IIF: 2 µg/mL	Life Technologies, D1306

Abbreviations: IIF, indirect immunofluorescence in retinal or optic-nerve sections.

Table S3: Comparison of retinal lengths estimated in reconstructed scanned images

Mouse age groups (no. of individual samples)	2 months (20)	8 months (18)	10 months (16)	12 months, untreated (20)	12 months, treated (20)
Retinal length normalized against the mean for the 2-month-old group	1 ± 0.015	1.117 ± 0.018	1.197 ± 0.02	1.185 ± 0.016	1.192 ± 0.015
P-value compared to 2-month-old mice		< 0.0001	< 0.0001	< 0.0001	< 0.0001
P-value for 12-month-old untreated vs 12-month-old treated mice					0.878

Retinal lengths are expressed as the means ± SEMs obtained for independent eyes in each group.

Table S4: Pairs of primers used in the RT-qPCR assays

Gene	Forward 5′–3′	Reverse 5′–3′
Ngb	CTCAGGCAAGGGAAGCATAG	CAGTTAGGTTTCCCCCAAAA
AAV-*NGB*	AGGCTATGTCACGAGGTTGG	GGGTAACCCTATGCAGTCGT
Atp6	CGTAATTACAGGCTTCCGACA	AGCTGTAAGCCGGACTGCTA
Brn3A	GAGGCCTATTTTGCCGTACA	CAGTAAGTGGCAGAGAATTTCA
Gfap	CCCGTTCTCTGGAAGACACT	CTTCAGGGCTGAGAGCAGTC